POLITECNICO DI TORINO

FACOLTÀ DI INGEGNERIA
Dipartimento di Ingegneria Meccanica e Aerospaziale

Corso di Laurea Magistrale in Ingegneria Biomedica

Tesi di Laurea Magistrale

ACL REHABILITATION: AN INERTIAL SENSORS-BASED APPROACH FOR FUNCTIONAL ASSESSMENT AND PROGRESS MONITORING

Candidato:
Sonia Bottone
Matr. S228320

Relatori:
Prof. Danilo Demarchi
Dr. Brendan O'Flynn

Correlatore:
Salvatore Tedesco

Anno Accademico 2017/2018

Contents

List of Figures

Abstract

The knee is the most stressful joint of the lower limb and the number of people affected by knee injuries is increasing.
One of the most common knee injuries involves the Anterior Cruciate Ligament (ACL) and its damage generally takes place during sport activities.
Rehabilitation procedures and programs after knee injuries have a macro- and micro-economic impact that is related to money provided by private healthcare institutions and money spent by patients to cure themselves, respectively. Furthermore, patients need to be monitored frequently by clinicians and experts over a long-time period.
The adverse impact on the economy, the lack of accuracy of clinical evaluations and the long-time monitoring that characterizes rehabilitation procedures lead to the necessity of developing low-cost, small, user-friendly and accurate wearable systems for knee health status assessment.

Nowadays, the gold-standard is represented by video-camera based systems. Despite the high accuracy, this technology is limited in long-term monitoring applications due to the lab constraints, the necessity of specific markers and trainings before using the device.
An alternative solution is offered by Inertial Sensor Measurement Units (IMUs), which showed to be accurate, cheap, and easy-to-use.

A comprehensive ACL assessment is developed using both qualitative and quantitative metrics. The former includes various indexes (e.g. KOOS, TUG, IKDC etc.) and is related to the clinical evaluation, while the latter is developed by extracting raw data from the IMUs and includes time-domain, frequency-domain and discrete-domain features.

To this purpose, this thesis analyses the application of Wireless Inertial Sensor Units for ACL assessment and proposes a method for evaluating the patients' progresses considering the widest range of features available in literature.

The first section contains an introduction about the ACL, rehabilitation programs that follow ACL breakage, and the evaluation of human motion. Furthermore, it is offered a detailed explanation of the inertial sensing system at the base of the proposed device, and the basic theoretical information which is currently present in literature useful for the knee status assessment. More in details, the last part of this section describes the theory and the method for extracting knee joint angles during typical exercises of ACLR, including the walking performances on a treadmill. In addition to the knee joint angles, temporal, spatial and frequency-domain parameters related to the gait are explained.

The second section described the algorithm developed in Matlab®. The proposed algorithm makes it possible to obtain not only the basic parameters, but a wide range of variables that helps in evaluating both the single repetition of an exercise and the whole performance. These variables are divided in 7 main categories: gait variables, statistical features, kinematic variables, info/theoretical and entropy-related features, jerk-based features, stability-related features and ROM-based features.

The third section offers an overview of the protocol applied during the sessions, descripts the performed scenarios (e.g. hamstring curl, flexion-extension, squat rotation, single leg wall slide and walking gait at different speeds) and proposes the application of a weighted K-means technique to evaluate the progresses of a single patient during ACLR through a single score indicator. The method for calculating the score is exposed and the results are compared to the expected trend.

The proposed method demonstrates to reduce the number of features initially computed, avoiding redundant and uninformative outcomes. Furthermore, the resulting trend of the score indicators helps in detecting a non-monotonic improvement of the patient along the rehabilitation program.

A different analysis that concerns the single leg wall slide scenario is additionally reported for having an estimation of the muscle control by studying the data distribution. This analysis shows a lower computational load in respect to the Fractal Dimension method available in literature and demonstrates that the patient is increasing the muscle control during the evaluated sessions.

In conclusion, the proposed algorithm gives a comprehensive and accurate outcome for analysing both the traditional scenarios (e.g. Hamstring Curl, Flexion-extension and walking sets) and new scenarios introduced in collaboration with two experts (e.g. Squat Rotation and Single Leg Wall Slide) and helps in overcoming the lack of an unambiguous method due to the intrinsic variability of the features.

This work confirmed that WIMUs are low-cost, small and user-friendly devices that are suitable for long-term monitoring applications in the biomechanical field and the method developed can be considered as an effective solution that can offer clinicians a detailed objective assessment that complements their subjective evaluation.

Sommario

Il numero di persone affette da patologie che coinvolgono l'articolazione del ginocchio è in continua crescita a causa dello stress che affligge quotidianamente le strutture anatomiche che la compongono.

Le ragioni possono essere essenzialmente di natura traumatica o degenerativa. Le ragioni di natura degenerativa sono legate a squilibri nei muscoli o nelle articolazioni (ad esempio, l'artrosi è una malattia degenerativa che riduce progressivamente la cartilagine articolare). Maggiormente legate allo stress e al movimento sono invece le patologie di natura traumatica. Queste ultime, infatti, sono generalmente risultanti da movimenti bruschi o scorretti durante attività sportive. In particolare, la patologia che manifestano più frequentemente gli atleti è la lesione del Legamento Crociato Anteriore (ACL).

È importante considerare che tali patologie necessitano di trattamenti costosi e a lungo termine (fino a 24 settimane).

La valutazione qualitativa effettuata da medici e fisioterapisti è basata sull'utilizzo di indici qualitativi (ad esempio, KOOS, IKDC, TUG etc.) e sull'impiego di strumenti poco accurati che non permettono di valutare la completa dinamica del movimento.

Il costo della riabilitazione, i periodici controlli, il lungo tempo di monitoraggio, e l'assenza di metodi di valutazione accurati rendono necessario lo studio di queste patologie al fine di sviluppare strumenti che permettano di migliorare tali aspetti.

I dispositivi proposti al giorno d'oggi e presenti sul mercato per valutare i progressi durante riabilitazione sono i sistemi di elettromagnetici, occasionalmente integrati con sensori di forza o di pressione, e i sistemi optoelettronici.

Nonostante l'elevata accuratezza offerta da tali dispositivi, il loro utilizzo resta limitato in applicazioni per monitoraggio a lungo termine. Le ragioni di tali limitazioni sono da ricercarsi nella necessità di utilizzare uno specifico ambiente di

laboratorio, determinati marker per l'identificazione del soggetto, e un'attrezzatura ingombrante per il cui utilizzo è necessario un training.
Una valida alternativa secondo la letteratura è rappresentata dai sensori inerziali, caratterizzati da una buona accuratezza, basso costo, e dimensioni notevolmente ridotte.

Per le motivazioni sopra riportate, questo lavoro si propone di ottimizzare un sistema per lo studio dell'ACL basato sull'utilizzo di sensori inerziali e sviluppa un metodo che calcoli, e successivamente selezioni, un certo numero di features rilevanti ai fini della valutazione del paziente.

La prima sezione contiene un'introduzione che include le cause dell'ACL, le caratteristiche di un programma di riabilitazione e le tecnologie utilizzate per la valutazione del movimento.

A seguire, è riportato lo State-of-the-art anticipato da una spiegazione dettagliata dei sensori inerziali alla base del dispositivo proposto.

L'ultima parte della sezione si concentra sul descrivere i metodi utilizzati per il calcolo degli angoli di flessione-estensione, varo-valgo e interno-esterno relativi all'articolazione del ginocchio (knee joint angles) durante l'esecuzione di tipici esercizi di riabilitazione e walking sets a diverse velocità.

La seconda sezione descrive l'algoritmo sviluppato in Matlab®.

Tale algoritmo permette di estrarre non soltanto i knee joint angles, ma una vasta gamma di features nel dominio del tempo e della frequenza che consentono di ottenere informazioni sul movimento legate sia all'esecuzione dell'esercizio nel complesso sia alla singola ripetizione.

Le features calcolate sono divise in 7 categorie principali: variabili del gait, variabili statistiche, variabili cinematiche, jerk-based features, variabili teoriche e associate

all'entropia, features legate alla stabilità e infine variabili legate al Range Of Motion (ROM).

La terza sezione offre un quadro complessivo del protocollo applicato durante lo studio del paziente e una descrizione degli esercizi eseguiti durante l'intero periodo di monitoraggio (9 mesi), ovvero hamstring curl, flexion-extension, squat rotation, single leg wall slide and walking gait.

Successivamente, è proposta l'applicazione di un algoritmo non supervisionato (weighted K-means) per definire uno score indicator che rispecchi l'andamento della riabilitazione.

L'algoritmo proposto è in grado di selezionare un sottoinsieme di features rispetto a quelle proposte inizialmente, evitando l'utilizzo di features ridonanti e poco informative che determinerebbero un costo computazionale eccessivo. Oltretutto, le features selezionate con tale metodo permettono di definire un andamento dello score indicator che rivela un miglioramento non monotonico del paziente durante tutto il periodo della riabilitazione.

Uno studio differente basato sull'analisi della distribuzione dei dati è applicato al single leg wall slide per avere una stima del controllo muscolare del paziente.

Questa analisi si rivela di facile implementazione e vantaggiosa dal punto di vista del costo computazione e permette di quantificare un miglioramento del controllo muscolare del quadricipite nel corso delle 4 sessioni analizzate.

Riassumendo, l'algoritmo proposto permette di identificare un quadro completo dello stato di salute del paziente e si rivela accurato sia negli esercizi tipicamente proposti in letteratura (quali Hamstring Curl, Flexion-extension and walking sets), sia in esercizi poco studiati ma proposti da esperti durante la riabilitazione (quali squat rotation e single leg wall slide).

La tecnica basata sulla definizione di uno score indicator permette, oltretutto, di oltrepassare le limitazioni date dall'assenza di un metodo di valutazione univoco principalmente determinato dalla variabilità intrinseca delle features.

In conclusione, questo lavoro conferma che i sensori inerziali sono strumenti economici, di dimensioni ridotte e accurati adatti ad applicazioni di monitoraggio a lungo termine per la riabilitazione di pazienti affetti da lesione dell'ACL. In aggiunta, il metodo proposto può essere considerato come una valida soluzione utile a offrire a medici e fisioterapisti dei parametri quantitativi da affiancare ai tradizionali strumenti e indici qualitativi.

CHAPTER 1

Human Motor Assessment

1.1 INTRODUCTION

Nowadays, an increasing number of people is undergoing a lower limb rehabilitation.

The leading causes of lower limb injuries are related to the age, gender, life-style and degenerative diseases.

The most vulnerable lower limb joints are the ankle and the knee.

Above all, knee is continuously stressed during daily work and sport activities. This stress could affect meniscus, patella and, to a greater extend, the ligaments [1].

The most common knee injury involves the Anterior Cruciate Ligament (ACL) [2].

Researches confirmed that the ACL can be raptured or damaged during sport activities, such as football, basket, skiing or basketball [2,3]. It was estimated a number of 80,000 to 250,000 ACL injuries per year in sportspersons [3].

Athletes with an injured ACL need to be treated with a non-surgical or surgical solution. The former consists in a simple immobilization of the leg, while the latter is linked to partial or total knee replacement.

Treatments and problems related to ACL are economically disadvantageous. To a recent review [4], more than 125000 ACL reconstruction were performed each year, leading to a cost that exceeds 1 billion of dollars. ACL consequences can be analysed in terms of micro and macro-economic impact. The “micro-economic” impact concerns money spent by a single patient to cure himself. On the other hand,

the "macro-economic" impact considers investments of public and private healthcare institutions.

The author reported in Table 1.1 a detailed description of factors and costs.

Table 1.1 Economic impact of the main items involved in ACL treatments [4].

Item	*Cost Range ($)*
ACL Reconstruction Implants	
Interference Screws	200-300
Tibial Fixation: other	200-500
Femoral Fixation: other	100-600
Allowgraft Cost	1400-3000
Total without allowgraft	600
Total with allowgraft	3100
ACL surgical cost	800
Post operative costs	
Physical therapy	4000-5000
Functional brace	800-1500
Cold Machine	300

ACL Rehabilitation (ACLR) programs aim to monitor the progress of patients in terms of muscle strength, bilateral and unilateral balance, coordination, range of motion and general mobility [2, 5, 6] (Figure 1.1).

The rehabilitation period is strictly dependent on individuals. Generally, patients after 2-3 months can perform normal daily activities (short-term rehab), while, a longer period from 6 to 9 months allows the return to sport (long-term rehab).

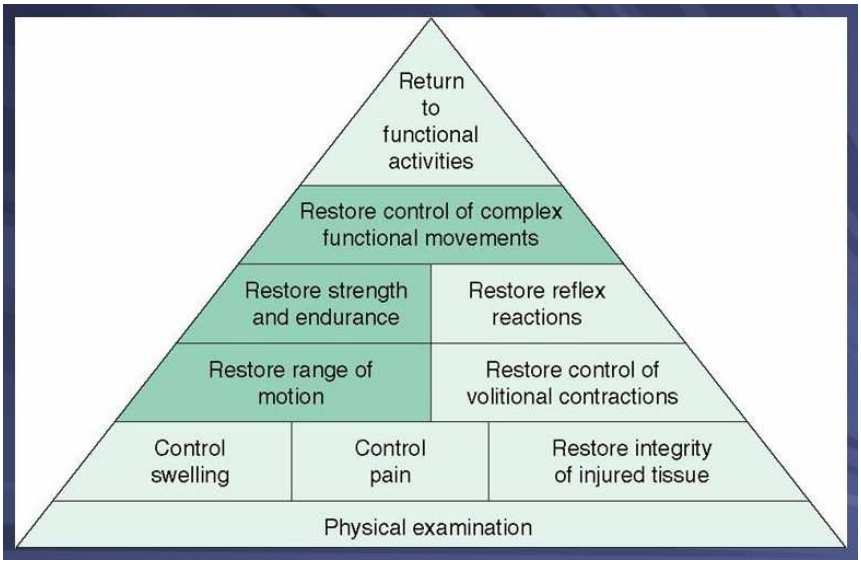

Figure 1.1: Hierarchy of rehabilitation goals [7].

A recent review [8] underlined the importance in observing both short-term and long-term rehab outcomes to assess full recovery of ACL patients. It was proved that only about 60% of patients get a full recovery, less than 60% return to sport activity, [3] and about 59% suffer for osteoarthritis of the knee. These statistics show the high socio-economic burden, especially related to the long-term complications. Hence, considering costs, the number of people and the long period of monitoring, it is essential to define methods and simple low-cost instruments that analyse short and long-term outcomes during Anterior Cruciate Ligament Rehabilitation (ACLR).

To this purpose, in this thesis is developed and optimized a method for ACL assessment by means of small low-cost Inertial Sensor Measurement Units (IMUs). Typical scenarios of ACLR are tested and evaluated in based on different categories of parameters. Finally, a method for extracting a single score indicator that helps the clinical analysis is proposed.

The rest of the thesis is outlined as follows. The human motor assessment and the gait analysis are described in Chapter 1. The explanation of Inertial Sensor Measurement Units and the State-Of-The-Art that concerns their application are illustrated in Chapter 2 and 3 respectively. The hardware platform and test protocol are defined in Chapter 4. The development of the algorithm for extracting the features and the assessment of the performance by means of a score indicator are described in Chapter 5 and 6. The results followed by an exhausted discussion about the outcomes are illustrated in Chapter 7. Finally, conclusions are reported in the last Chapter.

1.2 THE CAUSES OF ACL

The ACL consists in the rapture of one of the two ligament that link the femur (e.g. the thighbone) to the tibia (e.g. the shinbone) resulting in a less stabilization of the knee joint.

During sports and fitness activities the knee is particularly stresses and an ACL damage is likely to occur. The main manoeuvres that can cause ACL injuries are related to side-cutting movement, incorrect landing during jumps, unexpected braking, or a collision with another player during a match.

During the last decades, a considerable number of studies [3, 9-14] confirmed that female subjects are more prone to ACL injury: female-to-male ratio of ACL injury varies from 2 to 10.

The multifactorial reasons that caused this female tendency can be divided in three main categories: hormonal, anatomical and biomechanical. [13, 14]

On one hand, it was observed that a high presence of hormones could affect negatively the production of fibroblast and collagen. On the other hand, the wider female pelvis could determine less control on knee movements and patellofemoral disorders, leading to ACL.

From the biomechanical point of view, the main differences between male and female manoeuvres are linked to the neuromuscular activation. Female athletes had showed a stiffer knee, less knee flexion, and less hip flexion during their stand-on-feet exercises. Experts confirmed that the less is the flexion the more is the probability to get into valgus movements [15]. Consequently, a prospective study defined knee valgus movements as primary predictors of ACL injury. [9]

People who are affected from an ACL injury are more subject to knee osteoarthritis. The knee osteoarthritis is a pathology in which the joint cartilage deteriorates leading to a rougher contact between the bones.

The risk of osteoarthrosis is related to both the severity of the injury and the type of treatment during the rehabilitation.

An educational program [9] based on appropriate muscular, power and strength control helped in optimize exercises and reducing the risk of ACL.

More specifically, these exercises aim to:

- increase the leg muscles and the core strength (e.g. hip, pelvis and lower abdomen);
- train the patient in jumping and landing properly;

- improve the technique for performing side-cutting movements.

Following these guidelines, this document highlights the effectiveness of this idea of training. The training was developed in collaboration with two experts and monitored the progression of rehabilitation in a young female patient.

Figure 1.2: Anterior Cruciate Ligament (ACL) damage [16].

1.3 REHABILITATION PROGRAMS

To many experts, the cornerstone of ACLR programs is offered by the publication "*Current Concepts for Anterior Cruciate Ligament Reconstruction: A Criterion–Based Rehabilitation Progression*" developed by Douglas et al. [17].

This document defines the ACLR program as a gradual process based on performing specific sets of exercises. Types of exercises, sets and number of repetitions change during weeks and are set by physiotherapists who observe the patients along the rehab period. These changes establish a ranking of goals that the patient should fulfil.

During rehab programs patients go through five main phases: preoperative, postoperative, progressive limb loading, unilateral load acceptance, and sport specific training tasks.

A pre-to-post surgery monitoring could help in understanding impairments, disabilities, or wrong postures during exercises that needs to be avoided or corrected to improve long-term outcome [8, 18].

Despite the peculiarity of several studies [18 -22], progresses during rehabilitation depend on individual, which means that the patient follows its own rehab path. To date, the rehab path grows gradually from the suggestions of physiotherapists, clinicians, or more in general, experts that observe the patient's progression.

The five phases (e.g. preoperative, postoperative, progressive limb loading, unilateral load acceptance, and sport specific training tasks) are generally referred to a period of the rehab program (for instance, the preoperative generally refers to weeks 1-2, the post-operative to weeks 3-6, and so on). On the other hand, it is important to highlight that these general considerations need to be fitted for patients. In other words, the duration of the periods depends on the ranking of goals previously mentioned: if the patient satisfies the requirement set per each phase, it is possible to move to the next phase (Tables 1.2 - 1.3).

Regarding the five phases, the details extracted from [2, 17] are reported in the next subparagraphs.

1.3.1 PREOPERATIVE

It is common procedure to avoid the surgery unless the patient obtains many preoperative requirements: minimal pain, swelling and inflammation response, full and symmetrical ROM, increased muscle strength, normal gait walk and neuromuscular control (more details shown in Table 1.2 and Table 1.3).

Immediately after the surgery, the patient should follow clear instructions that acts on reducing the post-surgical pain and on improving early recovery to decrease the possibility of complications along the rehab program.

1.3.2 POSTOPERATIVE

From this phase to the unilateral load acceptance the patient gradually acquires strength, balance, and coordination acquired during the preoperative phase and lost with the surgery.

After the surgery the patients could be affected by patellofemoral problems, alteration in gait pattern, arthrofibrosis, quad atrophy or inhibition. In order to avoid these problems, aggressive control of pain and swelling, multidirectional mobilization of the patella, cryotherapy, and recovery of passive and active ROM are suggested in addition to the traditional medications, exercises and post-surgical compression bands. Furthermore, a normal gait pattern without crutches should be achieved within 10 days to avoid quad weakness, patellofemoral pain, and instability of the knee.

1.3.3 PROGRESSIVE LIMB LOADING

This phase aims to increase the strength of quad and hamstring by suggesting isometric, isotonic and isokinetic exercises. In particular, isotonic exercises, in which the contracted muscle is shorten against a load, proved to be very suitable for increasing the quad strength without affecting knee pain and knee laxity. Furthermore, cryotherapy and multidirectional mobilization of the knee are still suggested for pain, swelling and inflammation relief, in the first case, and to gradually achieve full extension of the knee, in the second case.

Then, it is essential to act on neuromuscular control for avoiding loss of proprioception and the related long-term complications. To this purpose, the

patients start practicing with basic exercises based on training the dynamic balance. The suggestions about exercises generally involves gait without crutches to train the patient in performing a normal gait.

1.3.4 UNILATERAL LOAD ACCEPTANCE

The purpose of this phase is to increase the unilateral strength, coordination, and balance while keeping previous goals such as full ROM, low pain and swelling, and neuromuscular control. During this phase, the patient should perform plyometric exercises in addition to dynamic balance training exercises. The former, indeed, train the patients in getting more agility, a proper concentric contraction power of the muscle, and unilateral balance.

At the end of this phase the patient should be able to react quickly to stimulations (e.g. changes in directions, sudden breakings, mental distractions) demonstrating enough control and coordination.

1.3.5 SPORT SPECIFIC TRAINING TASKS

"Sport Specific training tasks" give athletes reaction and responsiveness in relation to a specific movement. The athlete must able to perform a correct movement in absence of a feed-forward mechanism brain-to-action. To this purpose, the patients perform agility training, sprinting tests, turning and cutting manoeuvres, or simply exercises in which multiple mental distraction are applied. These exercises let the patients achieve the optimal neuromuscular control, increase muscle strength, and improve arthrokinetic reflexes.

It was proved that changes in the attentional focus during ACLR influenced knee flexion angle, knee extension moment and peak vertical ground reaction force [29].

After increasing the attention of the brain, the patients should be able to react to unexpected manoeuvres with an improved muscle control.

Table 1.2: Rehabilitation program: phases 1-3, time-based and criteria-based constraints (criteria to be satisfies for starting the next phase).

Phases	Time-based constraints	Criteria-based constraints
Preoperative	Weeks 1-2	• Minimal swelling (circumference at the patella < 1 cm); • Full ROM (symmetrical), full extension and full quad; • Flexion greater than 120 degrees; • Normal gait walking; • IKDC questionnaire outcome respecting the normal values; • Low pain score; • Quad strength in the injured leg which is > 85-90% compared to the uninjured leg.
Post-operative	Weeks 3-6	• No increasing of pain; • Minimal swelling; • Full extension, and flexion greater than 90 degrees; • Good patellar mobility; • Enough quad strength to perform mini-squats (0-30 degrees) • Normal gait with or without crutches.
Progressive Limb Loading	Weeks 6-12	• Minimal pain and swelling • Full extension, flexion greater than 130 degrees; • Normal gait pattern without crutches; • Perform exercises of previous week and stair climbing with no difficulties; • IKDC questionnaire (greater than 65% of the normative values). • Quad strength in injured leg is >60% compared to uninvolved leg

Table 1.3: Rehabilitation program: phases 4-5, time-based and criteria-based constraints (criteria to be satisfies for starting the next phase).

Phases	Time-based constraints	Criteria-based constraints
Unilateral load acceptance	Weeks 12-24	• Absence of pain and swelling; • Max difference between legs < 10 degrees in performing flexion and extension of the knee; • IKDC questionnaire (greater than 70% in respect to the normative values); • Quadriceps and hamstring strength of the injured leg >75% compared to the uninjured side; • Difference between the legs in hamstring/quadriceps strength ratio is <15%; • Exercises of previous week are carried out properly with weights; • Difference in single-leg hop for distance/cross over hop/vertical hop is <5% between legs; • Perform squat with overall weight lifted is <10% down on pre-injury level.
Sport Specific Training Tasks	Weeks 3-6	• Quadriceps and hamstring strength >85-90% compared to the contralateral side. • Sprint braking test and Timing of the Illinois agility test respecting fixed values; • Difference between legs in hamstring/quadriceps strength ratio <15%; • Hamstring/quadriceps strength ratio in the involved leg is >55% in women and 60% in men; • Hop tests of injured side >85-90% compared to the uninjured side; • IKDC questionnaire (within 10-15th percentile of healthy gender-age matched subjects); • No pain or swelling, during sport-specific activities; • Balance and agility training with maximal duration and speed.

1.4 HUMAN MOTION ASSESSMENT

The evaluation of human motion is the base of the whole rehab program.

Methods to assess patients' progress are still challenging due to (i) intra and (ii) inter variance among groups of patients, (iii) the consideration of the movement in multiple degrees of freedom (DoF), and (iv) the wide range of systems proposed to date [23]. More in details:

(i) The intra-variance is related to the execution of a single patient: the same exercise is performed in different sessions altering factors, such as velocity, Range of Motion (ROM) or the way to perform a movement. Recent evaluations [19, 22] confirmed that a visual guidance while performing the exercise helped in obtaining a proper and more coherent execution.

(ii) The inter-variance considers the same exercise performed by groups of patients with different age, gender, weight, and height.

(iii) The human manoeuvres act in different planes. In order to make complete and reliable evaluations, it is essential to avoid systems that consider one degree of freedom.

(iv) Previous clinical studies [19, 20, 21, 23, 25] showed the lack of reliable and accurate metrics to define the human motion. Generally, the methodologies considered for the human motion assessment are divided in 3 categories: clinimetrics, lab-based systems, and wearable technologies.

The categories of systems that enable the human motion assessment are described in detail in the next subparagraphs.

1.4.1 CLINIMETRICS

The clinimetrics is the science of clinical assessment. The clinical assessment concerns the direct observation of patients using simple instruments (i.e. goniometers and inclinometers), quality scores/questionnaires, and, occasionally, an activity diary.

Goniometers (Figure 1.3) are low-cost simple systems that provide an evaluation of the ROM of a single body joint. This instrument is positioned by a clinician with respect to the joint axis, and it allows measurement in one degree of freedom and in static positions.

As expressed before, every evaluation needs to be coherent with the movement, and therefore, must be conducted with multi DoF systems. Furthermore, ACLR programs always include patient's dynamic exercises whose performances cannot be detected with a static measurement.

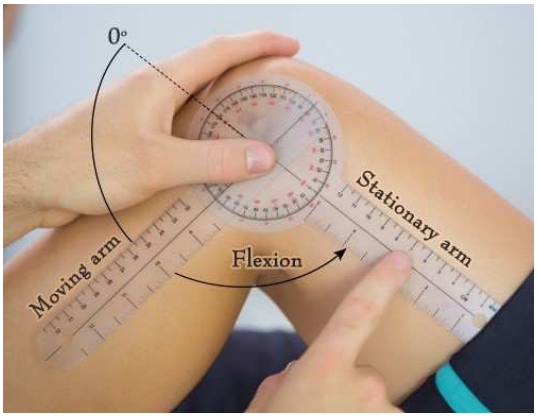

Figure 1.3: Evaluation of human motion using a traditional goniometer [26].

The use of other clinical instruments, such as electrogoniometers and inclinometers, lead to a more precise evaluation. Electrogoniometers avoid errors due to instrument alignment, while, inclinometers allow measurements in different planes

(Figure 1.4). Despite the fewer limits, both instruments still show difficulties in evaluating 3D dynamic movements.

Figure 1.4: Evaluation of human motion using an inclinometer [27].

Concerning scores estimations, several trials [19, 20, 21, 22, 24, 25] have provided a quality outcome during coaching activities.

The most common quality scores and questionnaires are resumed down below:

- *Qualitative Analysis of a Single Leg Loading (QALSL)*

  It defines criteria per each exercise included in the ACLR program. These criteria concerns knee motion, steadiness of the stance, trunk alignment, loss of horizontal plane etc. .

  When a single criterion is met the score assigned is 1, 0 otherwise. The total score is given by the sum of the scores of each criterion [2]. At the end of each session, the highest the total score, the worst the patient condition is.

- *International Knee Documentation Committee (IKDC)*

  It consists in ten questions divided in three categories: patients' symptoms, sport and daily activities, and knee motion before and after ACL rapture.

  The IKDC is the percentage of the difference between the highest and the lowest score, divided by the range of possible scores. All scores are then summed to get a single index. High values testify on good knee function levels and minor knee symptoms [21].

- *Time Up and Go Test (TUG)*

  It measures the time spent by the patient to rise from a chair, walk for 3 meters, turn around and go back to the chair. Normal ranges are around 11-20 seconds. When the test exceeds 30 seconds low dynamic stability is assessed.

- *Knee Circumference Measurement*

  It is based on measuring the knee circumference at the patella. Experts must be alerted when this value is more than 1 cm [2].

Other examples of quality metrics extracted from papers are the Western Ontario and McMaster Universities Osteoarthritis Index (WOMAC), Knee Injury and Osteoarthritis Outcome Score (KOOS), Development of the Patient Activation Measure (PAM), Health Resource Use Questionnaire, Stanford Self-Efficacy Questionnaire, Tegner Lysholm Scoring Scale (TLSS) and Body Mass Index (BMI).

For giving few examples, in [20] evaluated the effectiveness of using an activity diary and quality indexes, such as TUG and KOOS during an activity training.

Similarly, [22] compared the BMI to patient's satisfaction and exercise adherence. While, in [21] patient's progresses during treatment are studied through the IKDC and TLSS.

These studies have all highlighted that the use of quality score during rehab program can be used along with the standard instruments for increasing the satisfaction and the adherence of patients.

1.4.2 LAB-BASED SYSTEMS: HUMAN MOTION ANALYSIS GOLD STANDARD

A technical evaluation of 3D dynamic movement is obtained with the lab-based systems.

The most common lab-based devices proposed in literature are electromagnetic tracking systems, treadmills which occasionally integrates force platform, pressure mats and optoelectronic systems.

Electromagnetic Tracking systems (ETs) enable the identification of the position and orientation of several sensors in the 3D space [28].

The advantages in using such system is that they are quite inexpensive and do not need a well-lighted lab-environment for marker detection.

On the other hand, the ETs detects the location of the sensor through the emission of an electromagnetic field. Hence, this technology makes the analysis of dynamic movements possible and reliable. On the other hand, the presence of metal can affect adversely the measurements, and a further correction of the error is very time-consuming.

A second type of lab-based device is the instrumented treadmills (Figure 1.5). The whole system generally includes the treadmill, a high-speed camera, a work-station

for data elaboration, and occasionally markers and force platforms. These systems find their application in gait analysis for analysing the joint range of motion and for computing spatio-temporal parameters. Several brands have brought these system to the market, such as Medical Developments International (MDI), Bertec, AMTI, and Treadmetrics.

Despite the high-accuracy, the reliability and the customizable solution offered by these devices, the high-cost, the utilization limited to a lab space, and the bulky instrumentation are considered a great drawback that limits their use for at-home rehab.

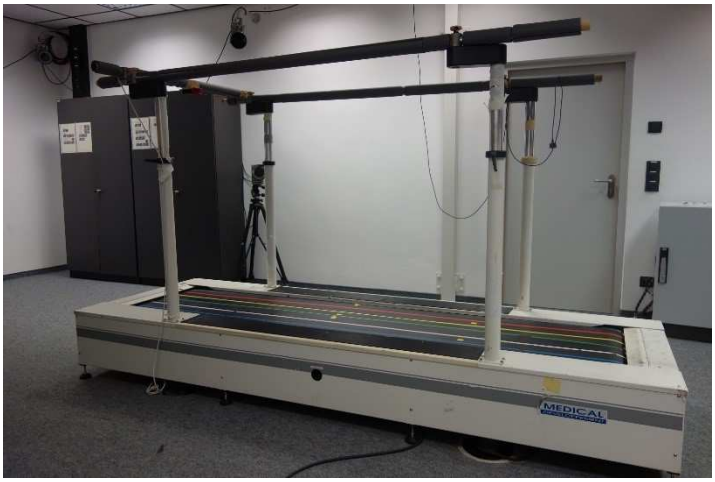

Figure 1.5: Instrumented treadmill with Kistler force sensor designed by MDI to measure ground reaction forces during human walking and running [29].

The category of video camera-based systems is considered the gold-standard of human motion analysis. The optoelectronic systems that are currently on the market are Vicon, Qualysis, Codamotion, Motek, and Biometrics [30].

These systems generally consist of several cameras, active or reflective markers placed on different positions of patients' body, and a workstation.

These devices reconstruct the subject model in based on the markers coordinates. Considering that markers can be hidden during subject motions, several cameras (instead of a single one) placed in different position of the lab help in detecting the

marker position during the development of the test. If the position of a specific marker is detected by multiple cameras, the redundancy is used to improve the accuracy of the reconstruction. Hence, this technology, compared to the others, offers the highest accuracy in the evaluation of the human motion in multiple DoF.

Unfortunately, the need of specific markers, the numerous lab-environment constraints (i.e. the level of the light for the markers detection), the training required to use the system, and the high cost and not portability limit the application of these systems to a restricted number of specialists (Figure 1.6).

Because of the evident drawbacks, none of these technologies is therefore suitable for at-home rehabilitation and long-term monitoring.

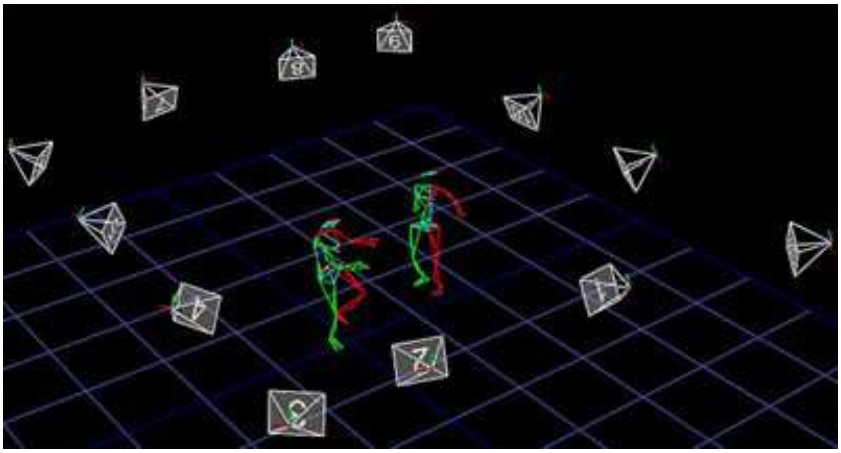

Figure 1.6: Video-camera based motion analysis using Vicon system [31].

1.4.3 WEARABLE TECHNOLOGIES: INERTIAL SENSORS MEASUREMENT UNITS

Nowadays, thanks to the expand of micro-electrical mechanical systems (MEMS), there is a growing trend towards to the application of Inertial Sensor Measurement Units (IMUs) in human motion analysis [23,30, 32, 33, 34].

Unlike the camera-based motion capture, these devices result to be environment-independent and avoid any issue related to camera set-up, resolutions, frame rate, etc. [30].

These advantages make the application of IMUs suitable for action or gesture recognition, gait identification, motion imitation in robotics, sport science, medical diagnosis, home-monitoring and rehabilitation [23].

The IMUs are electronic systems made by the combination of three sensors: an accelerometer, a gyroscope, and occasionally, a magnetometer. The accelerometer, the gyroscope and the magnetometer measure the acceleration, angular velocity and magnetic field in a specific location, respectively.

Using triaxial sensors, it is possible to assess the complete human motion of the part of the body on which the IMUs are placed over the 3D space.

Generally, raw data are extracted by means of a microcontroller on board, and then, saved on SD card or transmitted through a Wi-fi/BLE module.

The saved data are further processed to calculate the Euler angles (e.g. roll, pitch and yaw, these angles are referred to rotations around frontal, sagittal and frontal axis, respectively) and any other feature of interest.

This thesis proposes the use of four IMUs for monitoring weekly the ACLR of a young female patient.

The model of IMUs which is used to undertake this study is the Rev4 Wireless Inertial Measurement Unit (WIMU). The Rev4 WIMU is a 9-DoF, portable, low-cost device that was developed and validated at Tyndall National Institute.

The cost-effectiveness, the high accuracy, and the good performance give this body-worn system the flexibility to be considered as home-monitoring supporting device during ACLR. This could help in optimizing both the micro and macro-economic aspects linked to ACL.

During the test, the patient wears two WIMUs (the first on the thigh, and the second on the mid-shank) per leg by means of a stretchable velcro strap and performs many scenarios typical of ACLR (e.g. Hamstring Curl, Flexion-extension, Squat Rotation, Single Leg Wall Slide and walking sets at different speeds).

In particular, the pattern identified by the walking gait could reveals the presence of biomechanical irregularities that are due to an improper position on the foot during gait, to pathological conditions, or to sores in the back, ankle, knee and ligaments. For these reasons, it is considered as a key point to be evaluated during ACLR programs.

Thus, before reporting an overview of the State-of-the-art in IMUs in biomechanics an explanation of the principles of gait analysis is reported in the following sections.

1.5 GAIT ANALYSIS IN REHABILITATION

Gait Analysis is referred to the study of person's gait during walking or running and is considered as a key point to be evaluated during rehabilitation programs.

Pathological subjects show an irregular walking gait in which the posture can be fixed with orthotics devices, in case of structural problems, or coaching activities for improving the ACLR and reducing risk of ligament breakage [11,35].

During the walking gait the subject cyclically moves one foot after the other, hence, imaging to stop the scene in different frames, the subject can be seen with both foot on the ground or just one in contact while the other leg is moving. In a technical view, the former and the latter are called double and single support of the leg.

On the other hand, these frames identify what are known as gait phases: stance phase and swing phase. The gait phases, in turn, are defined by three temporal

instants of the gait which are known as Mid-Stance, Heel-Strike and Toe-off (Figure 1.7).

Furthermore, the combination between stance and swing phase returns the Gait Cycle Time (GCT).

Unlike the single support, the computation of the double support involves both legs and can be obtained by merging two sub-intervals called initial double-support and terminal double support. When the subject starts the walking gait with the left leg, the initial double support is extended from the left Heel-strike to the right Toe-off, similarly, the Terminal Double-support is extended from the right Heel-strike to the left Toe-off.

After giving a brief overview of all the parameters related the walking gait, more details are presented down below to allow a more comprehensive knowledge.

From this point, the notation used to define temporal instances of each leg is simply by inserting “right” or “left” in advance to the related word (for instance, right Toe-off, left Heel-strike etc.).

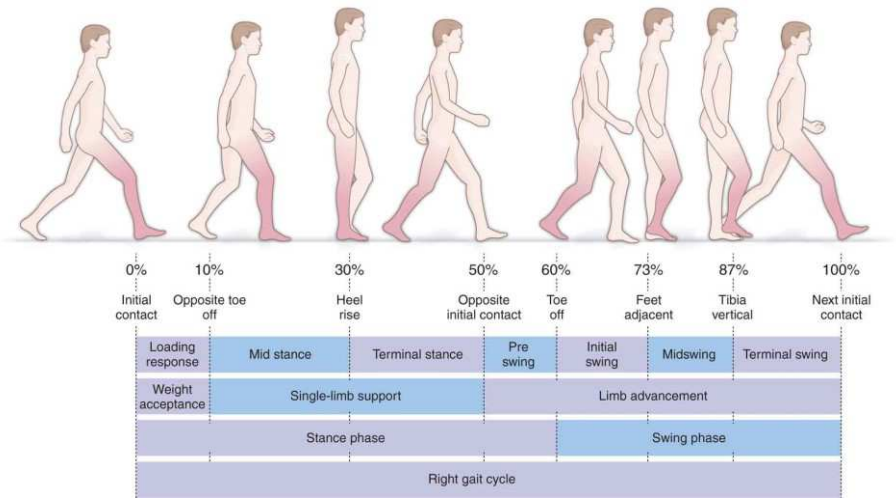

Figure 1.7: Representation of the walking gait phases and its definitions [36].

1.5.1 GAIT VARIABLES

As exposed before, the walking gait is identified by two phases (e.g. the stance phase and swing phase) and their combination between stance and swing phase gives an estimation of the GCT.

These variables can be defined as follows:

- The *stance phase* is the period of time when one leg bears the body weight in a single support by keeping one foot on the ground, and it generally represents the 60% of the whole gait cycle.
- The *swing phase* is the period of time while the subject is moving forward keeping one leg swinging in the air and it completes the remaining 40% of the gait cycle.
- The *GCT* is the period of time between consecutive contacts of the same foot. Hence, the gait cycle of a limb begins when the related foot contacts the ground and ends when the same foot touches the ground again.

The calculation of the temporal instants in both legs allows a further evaluation that involves the spatial parameters. The most informative spatial parameters related to the walking gait are the stride length, step length, stride speed, and the clearance.

1.5.2 GAIT TEMPORAL INSTANTS AND SPATIAL PARAMETERS

This paragraph gives an explanation of most parameters involved in the walking gait used for the assessment of the patient during rehab programs.

The temporal instants that determine the extension of the gait phases are called Heel-strike, Mid-stance and Toe-off.

The *Heel strike* (HS), also called initial contact, occurs when the feet contact the ground, the muscles (hip extensor, quadriceps, tibialis anterior) are contracted and the knee is bended around 15 degrees to stabilize the hip and absorb the shock.

The *Mid-stance* (MS), also called single limb support, marked the transition between double and single support. Hip extensors and quadriceps contract concentrically to allow the lifting of the limb until the shank is vertical in respect to the ground. The knee extension allows the verticalization of the limb and prevents the pelvis from falling at the next heel-strike.

The *Toe-off* (TO), also called initial swing, starts with the lifting of the limb, it continues with the cyclical muscles contraction to move forward the swinging limb, and it ends with the maximum knee flexion to allow a proper transfer of the body weight on the other limb.

After the calculation of the temporal instances, it is possible to extract the gait spatial intervals that have a definition in which they are involved.

The spatial parameters considered in this work are the Stride Length, Stride Speed and Clearance.

The *Stride Length* (SL) is limited by two consecutive placements of the same foot on the ground and can be considered as the double step length. The step length is the spatial interval which starts with the placement of one foot and ends with the placement of the opposite foot during the advancing movement of the subject in the walking gait. Unlike the step length, which could show different values for right and left leg, the values of the stride length should be the same along the advancement.

Then, the *Stride Speed* (SP) is detected as the distance over time. Generally, its values are around 89 m/min in males and 75 m/min in females.

Finally, the *Clearance* (CL) is considered as the maximum height reached by the foot during the swing phase [37]. Insufficient values of CL are often related to fall during walking (Figure 1.8).

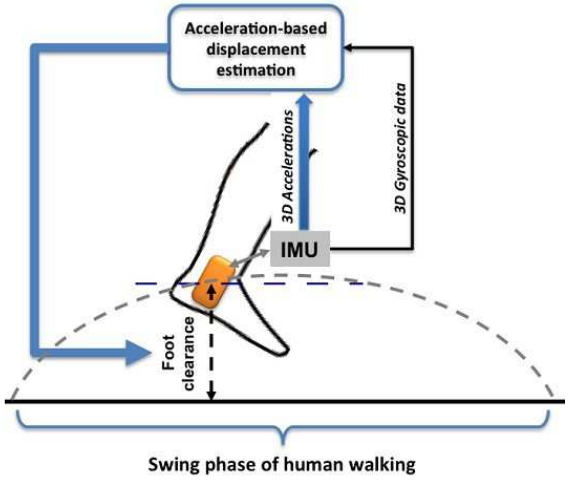

Figure 1.8: Graphical representation of the clearance detected by an IMU placed on the foot during walking gait [38].

CHAPTER 2

Inertial Sensing Measurement Units

2.1 IMUs BUILDING BLOCKS

To obtain a more precise evaluation of human motions during ACLR, the use of IMUs is taking over the application of video-camera based systems.

As mentioned in *Chapter 1*, IMUs are electromechanical devices based on the functioning of an accelerometer, a gyroscope, and, occasionally, a magnetometer [39,40,41]. The working principles of these sensors are described below.

2.1.1 ACCELEROMETERS

An *accelerometer* [42] is an electromechanical device that measures the acceleration forces (Figure 2.1). Measuring the static acceleration, it is possible to understand the position of the device in respect to the Earth, while, considering the dynamic acceleration the movement of the device is detected.

There are two types of accelerometers: piezoelectric accelerometer and low-impedance output accelerometer. The former is based on the squeezing of a piezoelectric crystal that causes an electrical charge directly dependent to the acceleration force. The latter converts the charge into low impedance voltage by means of tiny micro circuit and a FET transistor.

Accelerometers find their most common application in sensing free-fall, car crashes, or damages. As an example, they are used during the installation of the airbag in mechanical fields or for detecting the freefall of different objects in computer fields.

Due to its low-cost, size and integrability it is considered a valid alternative to other instruments in biomechanical applications.

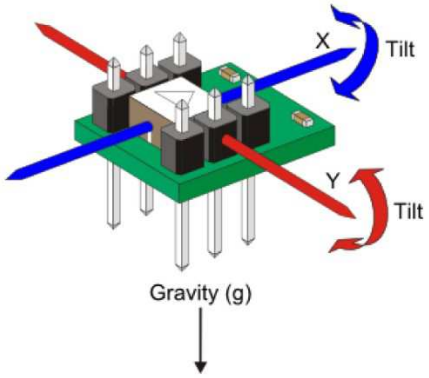

Figure 2.1: Accelerometer sensor [43].

2.1.2 GYROSCOPES

Gyroscopes are electromechanical devices that measure the angular velocity from the Coriolis force applied to a shaking element. They sense the change in orientation and in the rotational motion per unit of time [44].

More in details, the drive arm rotates in a defined direction. Then, a vertical vibration is produced by the Coriolis force which acts on the drive arms. In turn, the vertical vibration causes the bending of the stationary part producing motion in the sensing arms. This motion creates a potential difference from which angular velocity is first measured and then given in output as electrical signal. (Figure 2.2)

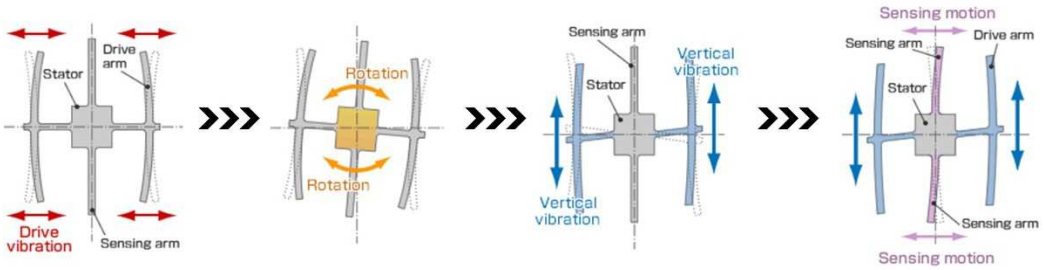

Figure 2.2: Schematic representation of the gyroscope principles [44]

With the development of MEMS, gyroscopes are becoming more compact finding new applications, such as shake detection in video-cameras, motion sensing in virtual reality, and car navigation. (Figure 2.3)

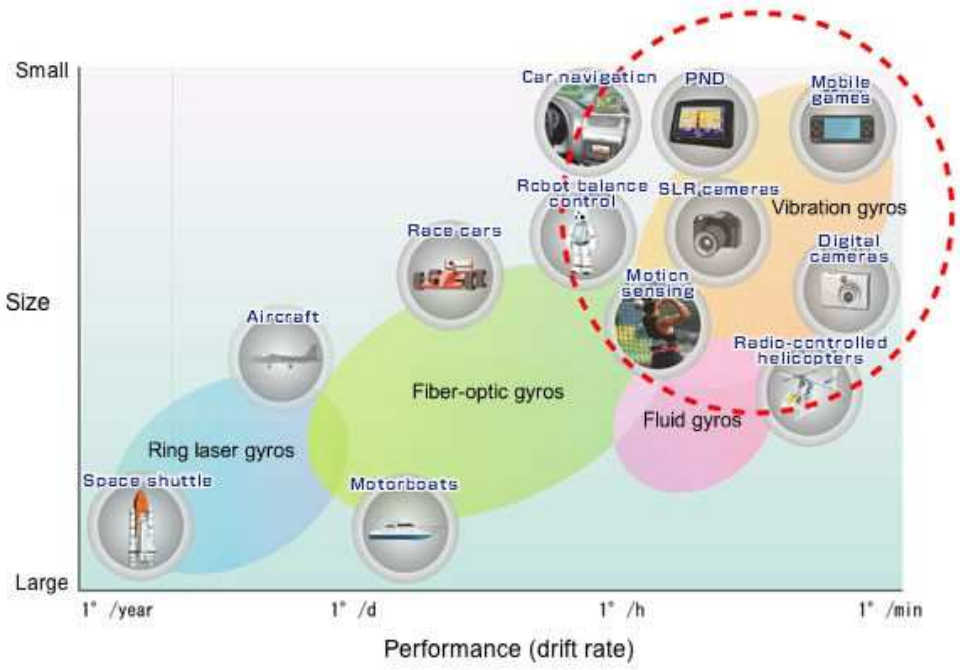

Figure 2.3: Main applications of gyroscope varying on size and performances [44].

2.1.3 MAGNETOMETERS

Magnetometers are devices that measures the magnetic field at a specific position (Figure 2.4). There are two types of magnetometers: vector magnetometers and scalar magnetometers.

Vector magnetometers sense the magnetic flux density value in the 3D space in a specific direction, while, scalar magnetometers sense the location and the amplitude of the vector of the magnetic field.

These systems can be inserted into IMUs to get more accurate results. Unfortunately, their calibration is challenging due to their sensibility to external magnetic fields. Both objects that create the magnetic field and metals of the environment could cause a distortion in the measurement. Considering these problems and following the confirmation of previous studies [45, 46], the use of magnetometer is not taken into account for this specific work, and the proposed IMU is mainly based on the functioning of accelerometer and gyroscope.

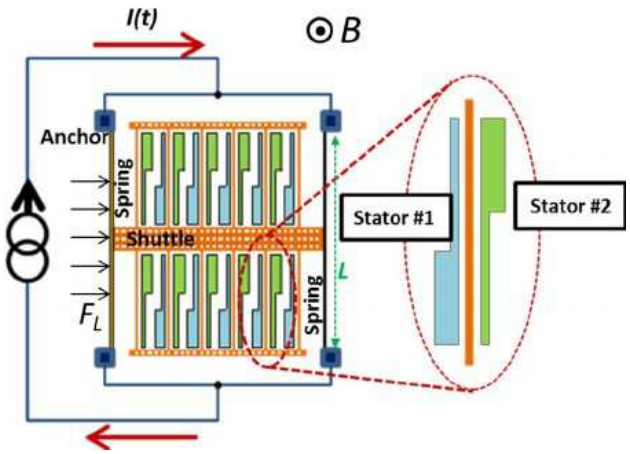

Figure 2.4: Schematic view of a Z -axis parallel-plate magnetometer. In presence of magnetic field, the suspended mass is subject to a Lorentz force, which further determines a displacement sensed through differential capacitors [47].

2.2 CLASSIFICATION AND ERRORS OF ACCELEROMETERS AND GYROSCOPES

Accelerometers and Gyroscopes can be defined by type, dimension, or field of application (Figure 2.5).

Lately, gyroscopes are applied in combination with accelerometers in inertial sensing platforms and are used for detecting the amount of angular velocity produced during sport activities [39,40,45].

In this study, a MEMS accelerometer and a MEMS gyroscope with a 3-axis dimension are inserted in an IMU for healthcare applications.

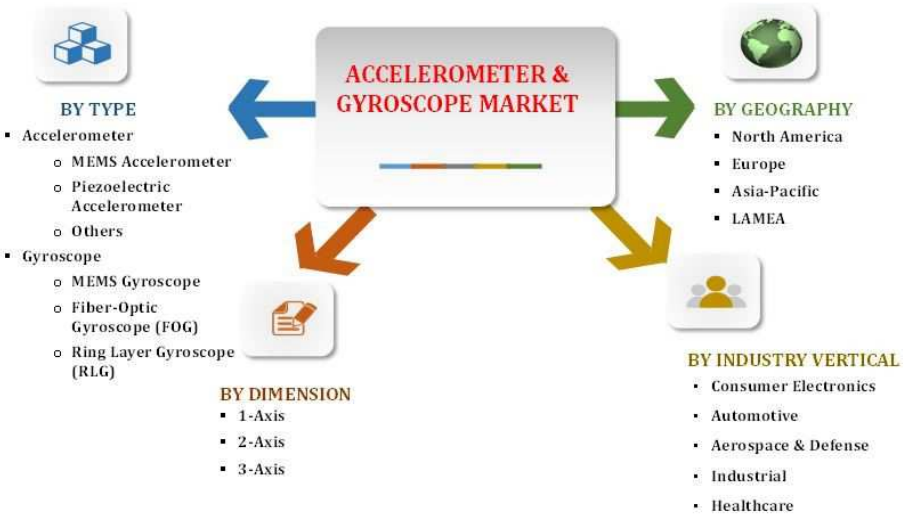

Figure 2.5: The categorization of accelerometer and gyroscope on the market [48].

In the application of gyroscopes and accelerometers the user must pay attention to both the starting conditions and the errors coming from the sensors [49]. These

errors, in fact, can lead to an imperfect identification of the object's location, or in biomechanical field, subject's location.

The main source of errors linked to the sensor are the bias, the scale factor and the noise (Figure 2.6).

The bias is the output that is obtained from the sensor when there is no input. The severity of this error depends on the type of system used (Figure 2.5), on the setup property, and the compensation of the system. The bias is represented by a constant offset and a factor, called bias drift, which varies on time and temperature. It is generally reported in the datasheets in units of mg, in the case of accelerometers, and in degrees/second, in the case of gyroscopes. The latter is more affected by this type of error, thus, the integration of data can cause a wrong estimation of the orientation.

The scale factor considers the ratio of change of the output in respect to the input ($K = S/I$, where S is the output, and I is the true input). Modifying the range of the input, it defines the slope of the least squared fitted line of the output data. This error is reduced during the calibration phase.

Finally, the noise could adversely affect the measurement and, therefore, it should be reduced.

In order to obtain parameters that reflect a realistic behaviour of the subject, the proposed algorithm combined the output of the accelerometer and the gyroscope gaining a higher accuracy in respect to the use of a single sensor.

In particular, the accelerometer is used for identifying the behaviour of the movement and the gyroscope is used for estimating the change in orientation and in the rotational motion per unit of time. Hence, this combination limits, on one hand, the noise of the signal taken from the accelerometer, on the other hand, it limits the bias drift typical of gyroscopes (Figure 2.7).

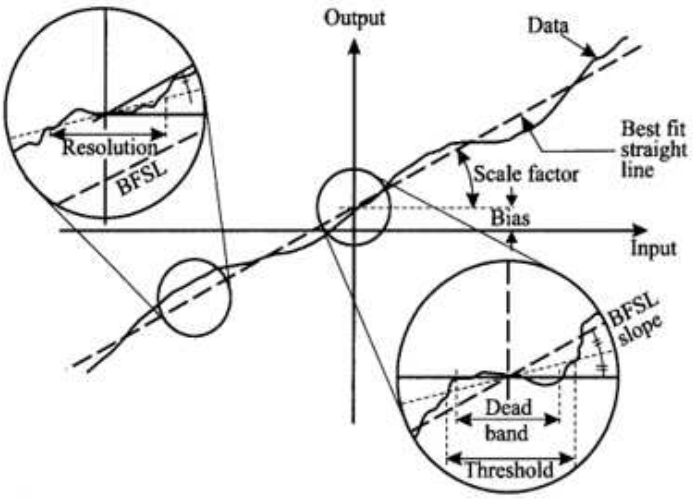

Figure 2.6: Schematic representation of all the error that can affect the measurement of accelerometers and gyroscopes [49].

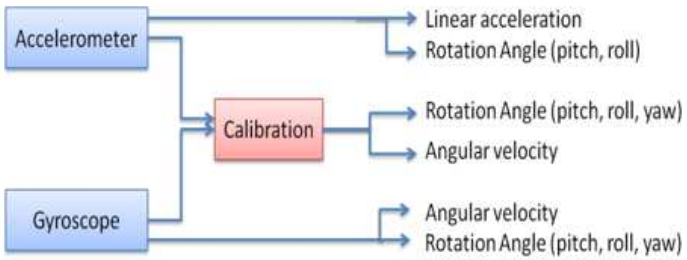

Figure 2.7: Combination between the output of the accelerometer and the gyroscope in order to gain a higher accuracy in respect to the use of a single sensor [46].

This trial tested, therefore, the combination between a triaxial accelerometer and gyroscope for monitoring the patient's progress during ACLR. The raw data taken from both sensors are used for extracting, first, the Euler Angles, and then, several statistical, time-domain, frequency-domain and info-theoretical features.

The explanation of the algorithm in which these parameters are calculated is anticipated by an overview of the state-of-the-art that analyses both the use of IMUs in biomechanics for the knee joint angles calculation and the gait assessment.

CHAPTER 3

Literature Review

To date, several studies proposed the use of IMUs in biomechanical fields. Different type of pathologies, methods and metric have been used for patients' health status assessment.

In the next section a brief overview of the latest applications of IMUs in biomechanics. It is shown particular attention is given to the lower limbs, because of their high stress. Then, the latest approaches to extract the basic parameters for starting the assessment of lower limb performances are also reported.

3.1 STATE-OF-THE-ART OF IMUs IN BIOMECHANICS

A wide range of inertial measurements have been proposed in literature.

Many of these are focused on a single movement or exercise. Johnston et al. [50] demonstrated that a single IMU in the lumbar area is sufficient for classifying pre and post-fatigue balance in Y Balance Tests. Differently from [50], Mo et al. [33] needed 5 IMUs placed on pelvis, on both shank and on foot to analyse the accuracy of two methods (e.g. S- and M-methods) to detect gait events at two running speeds. They concluded that the estimation of toe-off and initial contact is estimated with M-method and S-method, respectively, and the combination between the two allows a better prediction of stance duration.

In the meantime, the University of Waterloo [39] proposed the use of IMUs for an automated rehabilitation system in which patients' performances are evaluated with and without an exercise guidance during flexion-extension of the knee. This work proved the utility of visual feedback and guidance during the performance of rehab exercises.

Then, [41] and [51] evaluated whether IMUs are suitable to discriminate the correct execution of flexion-extension and lunges, respectively, and assessed that a single IMU is capable to differentiate correct and incorrect exercise performances (Figure 3.1).

Other studies are focused on improving the assessment of specific pathologies during different types of rehabilitation programs. Bonora et al. [32] validated a previous method for assessing the balance during the anticipatory gait adjustment prior to Parkinsonians' walking phase by positioning three IMUs, two on shins and one on the lower back. Teague et al. [34] undertook a knee health assessment by measuring acoustical emissions during three types of exercises. The acoustic sensing and knee joint angles calculation are realized by means of two contact microphones and two IMUs, respectively.

In alternative to the systems mentioned above, it is a common procedure to combine IMUs and other devices to improve the accuracy of results. For example, Spasojević et al. [40] developed a novel approach for supporting experts during Parkinson's rehabilitation combining both IMUs and Visual systems and extracting movement performance indicators from different exercises, walking included. The suggested system showed to be suitable for at-home rehab and supports clinical diagnosis with reduced subjectivity and imprecision.

Figure 3.1: An example of lower limb assessment reported in [51] which used 5 IMUs. One sensor is placed in the spinous process of the 5th lumbar vertebra, two at the mid-point of both femurs on the lateral surface and the remaining two on the shank of both legs.

3.2 KNEE JOINT ANGLES CALCULATION

The starting point of the majority of papers reported in the previous paragraph is the calculation of knee joint angles. This calculation is considered the cornerstone of the lower limb assessment and rehabilitation programs in which IMUs are involved. It basically consists in giving an estimation of the segments' motion by placing one or a multiple set of IMUs in proximity of the joints.

As reported in *Chapter 2*, the use of accelerometers and gyroscopes sometimes is supported by magnetometers to give information about azimuth and the horizontal plane.

So far, the use of the both inertial and magnetic sensors has been proposed in many studies and the most accurate method is based on the Kalman filter to estimate the orientation quaternion of the segments.

In literature [52] it has been proposed the use of magnetometer to obtain information incline that combined with the gravity vector of the accelerometer realising a strapdown integration on inertial acceleration. They showed a more accurate identification of the knee joint angles when applying magnetometers in addition to accelerometers. As a drawback, the magnetometer is subject to local fluctuations of the Earth's magnetic field due to the presence of surrounding ferromagnetic materials as exposed in Paragraph 2.1.3.

More recently, in [53] has been studied a system that includes magnetometers for extracting joint angles in gesture recognition. The signals taken from 3D-sensors have been filtered to remove high frequency noise and the segments orientation was computed using a gradient descent algorithm. This study confirmed that the application of such systems is limited to the rough assumption of homogenous magnetic field, which is very far from the real scenarios.

A research [54] has evaluated the reliability of a new systems made by the combination between e-textiles goniometer and tri-axial sensor for human motion analysis. A Kalman filter is the method used to measure the flexion-extension angle of the knee during different scenarios (e.g. monopodalic flexions and walking at different speeds). The proposed method showed an improved angular estimation compared to the results in applying textile goniometer and accelerometer, separately.

As a drawback, it revealed to be very intricate and the implementation of Kalman Filter led to high-computational load.

An alternative to the Kalman Filter is offered by [55], which proposed the combination between accelerometers and gyroscope for applying a direction integration of the signal, known as "strapdown integration", during sit-to stand exercises. It mainly consists in using the accelerometer during slow-moving scenarios, replacing it with gyroscope in faster scenarios when the variance of the accelerometers overcome a threshold. This shows to limit the noise that affected accelerometer and the bias drift typical of gyroscopes.

In [41] a three-link method that considers the application of IMUs without magnetic sensors for estimating both knee and ankle joint angles. This method is based on attaching an IMU on the subject's chest and it calculates the angles during the extension phase of stand-up motions.

The proposed algorithm needs the set of many variables and need the manual measurement of several parameters, such as the length of the trunk or thigh, that restricts its application.

To the above considerations for calculating knee joint angles it suggested to:

- avoid assumptions about the use of magnetometers;
- reduce the computational time;
- limit the set up to the lowest number of parameters and search for solution that does not require a high computational load.

To these purposes, in this work the magnetometer is not taken into account and the raw data of both accelerometer and gyroscope are used in combination to improve the accuracy of results.

Then, to reduce the computational time that characterizes the application of the Kalman Filter, a Gradient Descendant technique is used for extracting the Euler Angles.

Finally, the set-up is limited to one parameter that corresponds to the distance between the ground and the sensor placed on the shank, useful for avoiding the rough assumption on the initial velocity (e.g. initial velocity equal to zero) and improving the accuracy of the spatial parameters during the walking gait *(see Chapter 6)*.

3.3 GAIT ANALYSIS IN LITERATURE

Following the explanation of *Chapter 1* that concerns the basics of gait analysis, this section offers an overview about the recent studies that aim to obtain a gait assessment by means of IMUs. The main objects of these studies are: (i) assessment of balance during gait, (ii) evaluating gait symmetry, (iii) prediction of gait temporal instants, (iv) estimation of walking speed, and (v) improve the accuracy of the detected parameters by means of machine learning.

As previously mentioned, an example of balance estimation is offered by [32], in which three IMUs have been used for data recording during the anticipatory gait adjustment that anticipate the Parkinsonians' walking phase. A similar evaluation has been developed in [56] in which IMUs have been used to track the upper body motion during walking tests. More specifically, this study compared four methods for aligning the IMUs in respect to the global reference for correcting the raw signal of the acceleration.

Another object is proposed in [57]. This study is an example of gait symmetry assessment, in which a quantitative assessment of gait symmetry for defining the health status of patients affected by hip-replacement has been provided. More specifically, it has proposed a symbolic-based symmetry measure that quantify the similarity between right and left side, making the measurements independent from the speed at which the exercise is performed.

On the other hand, in [58] an application of IMUs, in addition to pressure-sensitive insoles, for detecting gait initiation and termination has been developed. The proposed algorithm has detected two instances called gait onset and toe-off by segmenting the gait into steps and applying a supervised machine learning technique. Better results are shown for detecting the gait initiation in respect to the termination (well-predicted in the 80% of the trials).

Regarding gait parameters, in [59] has been proved that it is possible to estimate the walking speed by means of IMUs placed on the shank and on the feet for detecting the single stride cycles. More specifically, the walking speed is calculated by integrating the angular velocity and linear acceleration extracted from the sensors.

Another example the computation of its parameters has been offered in [60]. This analysis has provided a wide range of parameters related to the gait (e.g. cadence, ambulation time, step time, gait cycle time, stance and swing phase time, simple and double support time) by extracting the raw data from two accelerometers placed on the ankles. Then, a Bayesian classifier is applied to optimize the obtained results by distinguishing between step and non-step.

This thesis tries to include all the mentioned objects. The balance estimation is given by computing the foot clearance, that can be defined as primary prediction of falls during gait. Then, the recorded gait sessions are segmented in order to detect temporal instants and the related spatio-temporal parameters, including symmetry and stride speed. Finally, an unsupervised machine learning technique (e.g. K-means) is applied for having an estimation about right and left differences and defining a score indicator.

CHAPTER 4

HW platform and data collection protocol

As exposed in *Chapter 1,* the gold-standard technologies can offer a great quantity of information regarding the human motion with the highest accuracy, but important limits such as the high cost or the need of a lab environment.

For these reasons these devices revealed to be unsuitable for a long-term monitoring of patient after the knee surgery.

The inertial sensing platform represent a more practical solution at a small-size and low-cost.

4.1 THE MONITORING SYSTEM

The monitoring system used in this work is made by four Wireless Inertial Measurement Units (WIMUs) developed at Tyndall National Institute.

Each leg is equipped with two WIMUs, one placed on the thigh and the other placed on the shank (Figure 4.1).

Figure 4.1: WIMU developed at Tyndall National Institute [61].

Each WIMU is made by the following components [61]:

- the motion tracking device;
- a high-performing micro processing unit (MCU);
- a Bluetooth complaint module (BLE);
- A rechargeable battery.

In addition to the main components, the platform is equipped with a USB connector, a battery charger, three LEDs for the battery monitoring, a power switch for starting the data recording, 1 Mb of flash memory and 192 plus 4 Kb of SRAM, several enhanced I/Os and peripherals, and other communication interfaces.

The dimension of the platform is 44 x 30 x 8 mm without battery.

Finally, the whole system is enclosed in a 3D printed case and fixed to a stretchable velcro strap.

4.1.1 THE MOTION TRACKING DEVICE

The motion tracking device is composed by an accelerometer and a gyroscope included in a MPU-9250, Invensense. [62].

The Invensense MPU-9250 is a 9-axis device (Figure 4.2) that offers optimal motion performances at the smallest size (size reduced of 44% in respect to other devices on the market).

This device revealed to be suitable for different applications that aims to evaluate the motion, such as motion-based game controllers and wearable sensors for health, fitness and sports.

Both accelerometer and gyroscope present a digital-output with a user-programmable full-scale range whose highest values are 16g and 2000°/sec, respectively. In addition to the high range, the power consumption is very low, only 9,3 μA.

Figure 4.2: The Invensense MPU-9250 is a 9-axis motion-tracking device [62].

4.1.2 THE MICROPROCESSING UNIT

This sensing platform is wired to the high-performance microprocessor ARM Cortex-M4 through a I2C communication [63].

The Cortex-M4 microprocessor reaches 32-bit performance with low power consumption and an operating frequency up to 180 Hz (Figure 4.3).

The Memory Protection Unit (MPU) improves the software reliability giving to each module the access only to defined areas. This help in avoiding problems of overwriting clinical data due to unexpected accesses. Then, it additionally shows a Floating Point Unit (FPU) that enables the device in obtaining accelerated single-precision floating-point operation.

The high efficiency, the reliability, low-power consumption, low cost and easy-of-use satisfy a large variety of market and make it a flexible solution also for targeting motor control.

Figure 4.3: The Cortex-M4 processor part of the STM32F0407 family produced by STMicroelectronics [64].

4.1.3 DATA COLLECTION

The data captured from the sensor can be transmitted using a wireless transmission or recording them at a sampling rate of 250 Hz on a removable Micro SD card.

The wireless transmission is obtained by means of a Bluetooth-complaint module, Broadcom BCM20737S. This system integrates an ARM C3 microcontroller unit, radio frequency and embedded Bluetooth Smart Stack achieving single mode low-energy solutions.

4.2 PATIENT DETAILS

The injured subject tested in this study is a young female athlete, whose details are shown in Table 4.1, that underwent a knee surgery for reconstruction of the left anterior cruciate ligament.

This information is inserted in the section “Test details” included in the Graphic User Interface (GUI) described in detail in *Chapter 5*.

Overcoming the limitation of recent studies which analysed only the starting part of rehabilitation process, this analysis starts in the pre-surgery phase and monitors weekly the patient during the rehab covering a period of nine months. Thus, it is possible to evaluate both patient's improvement during the rehab program and the occasional long-term complications.

Tab.4.1 Patient personal details

Name	*Niamh*
Surname	*Creedon*
Age	*26*
Weight	*57 Kg*
Height	*167*

Tab.4.2 Timetable of the trial.

Start date of the trial:	*23.03.2017*
End date of the trial:	*14.12.2017*
Injury date:	*22.01.2017*
Surgery date:	*04.04.2017*
Frequency of capturing data:	*Weekly*

4.3 PROTOCOL OF THE DATA CAPTURE

Before starting the evaluation of the patient in different scenarios, the body-worn inertial sensors have been placed laterally on the thigh and on the anterior tibia by means of stretchable velcro straps (Figure 4.4).

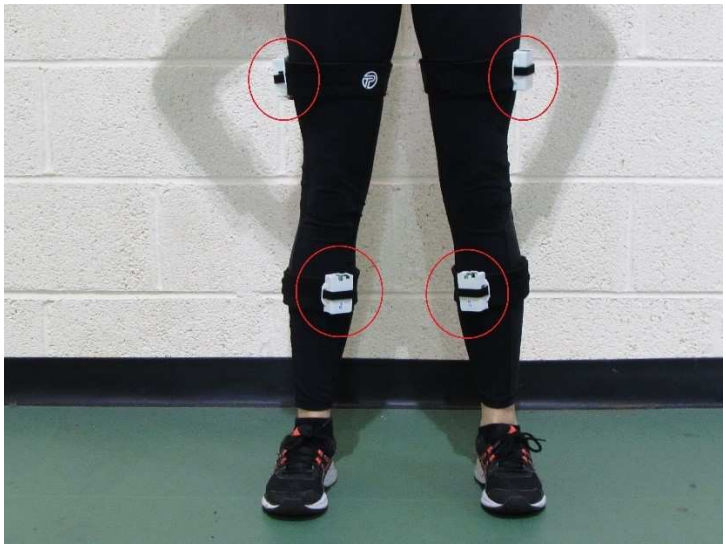

Figure 4.4: The 4 WIMU (circled in red) are placed by means of stretchable Velcro straps on the shank and thigh of each leg.

The protocol has been developed with the suggestion of two experts, and generally reflects the activities assigned by clinicians for at-home ACLR.

The different types of scenarios included in this protocol are Hamstring Curl, Flexion-extension, Walking sets, Squat rotation, and Single leg wall slide. During each scenario a defined number of repetition is performed to improve the quality of results.

The exercises have been introduced gradually during rehabilitation taking into account the standard of rehab protocols [1]. Generally, Squat rotation and Single leg wall slide cannot be tested until the patient shows full range of motion of the knee and enough single leg strength. For these reasons, these scenarios have been analysed only in the last part of the rehab monitoring program.

Furthermore, each scenario is anticipated by a squat performed by the subject to allow the data synchronization of the WIMU (see *Chapter 5*).

In the following subparagraph a brief explanation of each scenario and the associated technique is reported.

4.3.1 HAMSTRING CURL

The hamstring curl is based on standing on one limb while bending the opposite knee to allow the heel movement to the gluteus.

This movement is repeated 15 times per 2 sets, with a little relaxation of muscles after each repetition in which the heel returns to the ground.

4.3.2 FLEXION-EXTENSION

In the flexion extension scenario the subject contracts the hamstring muscles and bends the knee in direction of the chest digging the heel into the ground [2].

This movement is repeated 15 times per 2 sets, distending the limb after each repetition in which the knee returns to the starting position.

4.3.3 WALKING SETS

The walking sets are performed by means of a treadmill at three different speeds: 3, 4 and 6 km/h. Per each speed are performed two sets (or trials) that last about 1 min.

4.3.4 SQUAT ROTATION

In this exercise the subject contracts quadriceps and gluteus, keeps the knee bended around 90 degrees, and performs frontal, lateral and hyper-extension of the knee, three times per each leg (Figure 4.5).

4.3.5 SINGLE LEG WALL SLIDE

In the squat wall slides the patient enhances the quadriceps and knee strength standing with the back leaning against a wall, keeping the foot about 30 cm from it,

and bending the knee about 90 degrees. Then, one leg is lifted while the opposite one stands for about 20 s. This set is repeated one time per each leg (Figure 4.6).

Figure 4.5: The patient while performing squat rotation. Stage 1: Bend the knee around ninety degrees. Stage 2-4: perform frontal, lateral and hyper-extension of the knee.

Figure 4.6: The patient while performing single leg wall slide. Stage 1 (lateral view): Bend the knee around ninety degrees. Stage 2 (frontal view): keep one leg lifted about 20 seconds.

After performing the set of exercises defined in each session, the raw data recorded in the four WIMU are extracted and elaborated for the computation of the knee joint angles, spatio-temporal parameters of gait and a varied set of features. A detailed explanation of the algorithm developed to achieve this purpose is reported in the next Chapters.

CHAPTER 5

Algorithm development

The algorithm is entirely developed in MATLAB® and includes four main stages:

- insertion of patient's personal information in the Graphic User Interface (GUI);
- knee joint angles and gait spatio-temporal parameters calculation,
- features extraction (e.g. kinematic, statistical, info-theoretical and entropy-related, ROM, and stability variables);
- the formulation of a distance metric followed by the application of a feature selection method for the calculation of the score indicator.

In the following section a detailed explanation of each stage is provided.

5.1 GRAPHIC USER INTERFACE

Before starting the calculation of the parameters, a GUI is created to insert the personal data of the patient and to select the specific type of exercise among all the ones performed in a single session (Figure 5.1). More specifically, there are three boxes, the *Personal Details* box contains personal details, such as name, surname, date of birth, gender, height, and weight, while the *Test Details* box concerns the test details and includes the date when data have been captured, the type of test, the number of trial, the number of record and the segment (see *Paragraph 4.3*).

The data recorded along a session are saved in '.txt' files whose names have a correspondence to each WIMU. Hence, the user needs to insert the number of IMUs in the specific section to load these files and convert them from '.txt' into '.mat'.

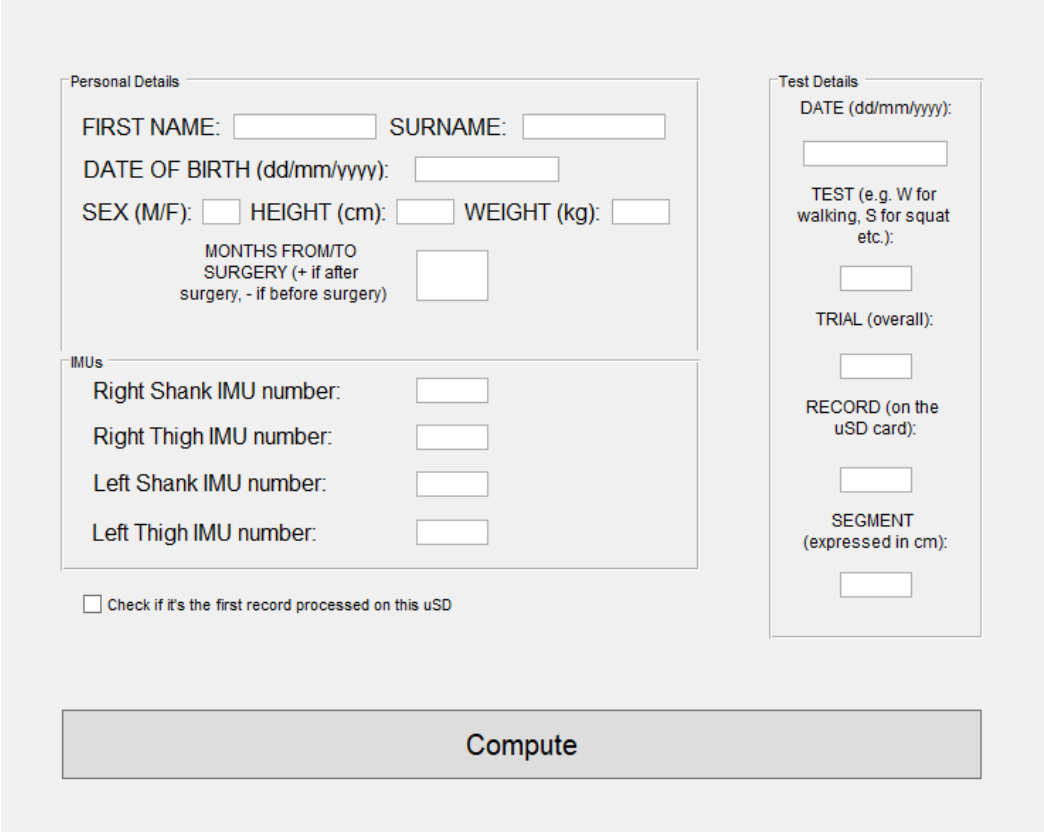

Figure 5.1: Graphic User Interface developed in Matlab®. The personal and test details of the patient are inserted on the top-left and right, respectively.

The personal details inserted in the GUI are then copied in an Excel Sheet to personalize the processing of the patient.

Regarding the *Test Details* box, (i) *Date* is useful for having the reference of a specific session when the data are saved in the personal folder, (ii) *Test* and *Trial* are used to differentiate the thresholds during the segmentation phase for the identification of repetitions/strides, (iii) *Record* has a correspondence to the order in which the exercises are recorded during the session and is used for selecting a

specific one, and (iv) *Segment* is used for avoiding the boundary condition of zero-velocity during the computation of spatial parameters.

5.2 KNEE JOINT ANGLES CALCULATION

The Knee Joint Angles Calculation starts with the import and conversion of the raw data into matrixes. The conversion of the raw data (in text format) into matrixes is realised by using the test information inserted in the GUI to isolate a single exercise from the others.

At the end of this stage of the algorithm the knee joint angles are calculated.

This stage can be further divided in four main steps:

- pre-processing and IMUs temporal alignment;
- conversion to the Joint Coordinate System (JCS);
- horizontal plane alignment;
- computation of 3D orientation for each IMU and conversion to Euler Angles.

5.2.1 PRE-PROCESSING AND IMUs ALIGNMENT

Considering that IMUs do not communicate to each other and their turning on/off is not simultaneous, a pre-processing phase is required to align the data collected from the four inertial sensors. The alignment is realised by asking the patient to perform a squat before each performance. Data are first filtered with a median and a low-pass filter to obtain an ultra-smooth curve. The smoothing is essential before starting the identification of a truthful squat in each IMUs.

More in detail, the chosen low-pass filter is a 2nd order Butterworth filter whose normalized cut-off frequency is set as the ratio between f_c and $f_s/2$ (where f_c and f_s are equal to 1.25 Hz and 250 Hz, respectively). This is applied to limit the white noise that affects the signal. One of the key benefit of this filter is related to its capability to minimize the distortion by processing the signal in both directions (e.g. forward and reverse).

It is likely that errors generally affecting these types of systems can lead to temporally-distant samples. For this reason, a second interpolation is acted to limit the distance between adjacent time-stamps when this distance overcomes a threshold value fixed at 0.025.

Then, the IMUs are aligned and resampled. The alignment is performed first between thigh and shank of the same leg and then between the two legs. The resampling is necessary for cutting all matrix to the same number of elements. The size is clearly considered as the minimum among the dimension of the four matrixes taken from the sensors.

5.2.2 CONVERSION TO THE JOINT COORDINATE SYSTEM (JCS)

In order to overcome the limitations due to the absence of a uniformed coordinate system, the JCS conversion is applied [67]. The JCS is generally for analysing the joint angles related to the human manoeuvres with a clinical relevance. For this reason, a conversion to conform the actual Joint Coordinate System to the JCS is applied for both right and left leg (Figure 5.2).

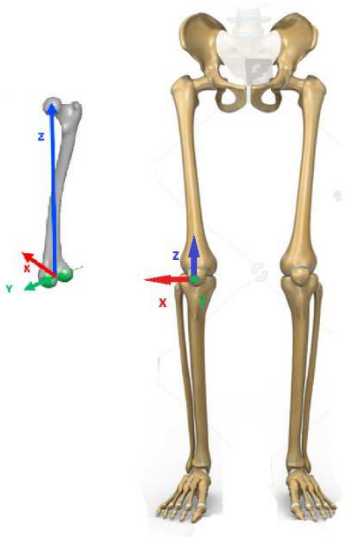

Figure 5.2: JCS reference: frontal and lateral view of lower limb inspired by [66].

5.2.3 ALIGNMENT ON THE HORIZONTAL PLANE

This stage is performed per each leg and it aims to spatially align the IMU of the shank with the IMU of the respective thigh.

Following the theory developed by Seel et. al [67] the knee can be considered as a hinge (Figure 5.3). More in details, the iterative algorithm proposed in [67] starts by modelling the lower limb as three segments connected by a spheroidal joint to which the IMUs are fixed. Both joint axis and position are first initialized randomly (by choosing values in a reasonable range), and then, updated by subtracting the Moore-Penrose-pseudoinverse. As a final outcome, a translation and rotation of the segment (respecting the kinematic constraints) is realized.

In this thesis, starting from the knowledge of angular velocities of both thigh and shank in random instants, this optimization algorithm is capable to obtain a rotation around the z-axis of the IMUs of the shank to align their x-axis in respect to the x-axis of the respective IMUs of the thigh. Considering the knee as a hinge, the IMUs

of the thigh are considered already aligned, in fact, their x axis reflects the rotation of the knee.

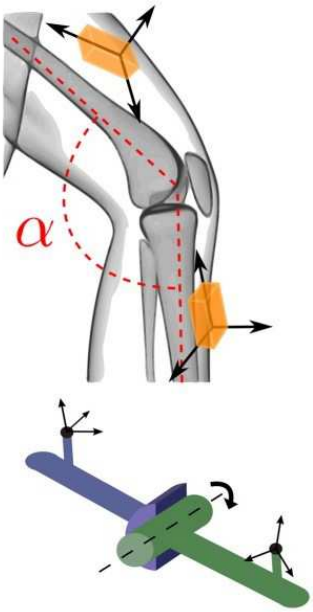

Figure 5.3: The knee considered as a hinge. The triaxial coordinate systems on each segment reflect the location of the IMUs on thigh and shank [68].

5.2.4 COMPUTATION OF 3D ORIENTATION AND CONVERSION TO EULER ANGLES

This stage returns the Euler Angles of the knee around x-, y- and z-axis. More specifically, it is calculated the local 3D orientation of the sensor in respect to the global reference.

The local orientation is extracted separately from accelerometer data and gyroscope data through a Gradient Descendent Algorithm, then both results are combined by means of a fusion filter that finds a robust solution overcoming both gyroscope and accelerometer-related errors.

This solution allows users to avoid the typical drift of the gyroscope that characterize low frequency signal and the high frequency noise of the accelerometer, revealing to be a good and simple alternative to the intricate Kalman filter. Put simply, the accelerometer and gyroscope data are filtered through low-pass filter and high-pass filter, respectively.

This fusion filter is modelled as follows:

$$\boldsymbol{q}_{filt,t} = \alpha * \boldsymbol{q}_{\boldsymbol{gyr,t}} + (1-\alpha) * \boldsymbol{q}_{\boldsymbol{acc,t}} \quad (5.1)$$

Where $q_{filt,t}$ is the output of the single observation and a 4x1 vector with elements [q_1, q_2, q_3, q_4], $q_{gyr,t}$ and $q_{acc,t}$ the quaternions calculated and normalized for accelerometer and gyroscope respectively, and α is in the weight that select the contribute of the sensors.

Once the output of the fusion filter is obtained, this value is converted into Euler Angles of the sensor using the following definitions [69]:

$$\phi = \tan^{-1}\left(\frac{2(q1*q2+q3*q4}{1-2(1-2(q_2^2+q_3^2)}\right) \quad (5.2)$$

$$\theta = \sin^{-1}\left(2(q1*q3-q4*q2)\right) \quad (5.3)$$

$$\phi = \tan^{-1}\left(\frac{2(q1*q4+q3*q2}{1-2(1-2(q_3^2+q_4^2)}\right) \quad (5.4)$$

Where q_1, q_2, q_3, q_4 are the elements contained in $q_{filt,t}$ on the respective axis, and φ, θ, ψ are the Euler joint angles (roll, pitch, and yaw) extracted for both shank and thigh. These angles lead to the calculation of the flexion-extension ($\emptyset_{FE}$), varus-valgus (θ_{VV}) and internal-external angles (ψ_{IE}), respectively, by combining the values of thigh and shank. Hence, to calculate the knee joint angles in respect to

both legs the values obtained on the thigh are subtracted to the ones obtained on the shank, as follows:

$$\emptyset_{FE} = \emptyset_{thigh} - \emptyset_{shank} \quad (5.5)$$

$$\theta_{VV} = \theta_{thigh} - \theta_{shank} \quad (5.6)$$

$$\psi_{IE} = \psi_{thigh} - \psi_{shank} \quad (5.7)$$

5.3 GAIT SPATIO-TEMPORAL PARAMETERS

The second stage of the algorithm is the definition and calculation of the spatio-temporal parameters related to the walking gait. An overview of gait analysis at the base of human locomotion, with attention to gait instances, anticipated the computation of gait spatio-temporal parameters in *Chapter 1* to provide a deeper understanding for the reader.

5.3.1 GAIT TEMPORAL INSTANCES

The implementation of the temporal instances relies on the shape of the curve that characterizes the gait pattern.

In Figure 5.4 is reported the angular rate around the frontal x axis of the gyroscope of a single cycle. The Heel-Strike, Mid-Stance, and Toe-off represents three inflexion points of the signal.

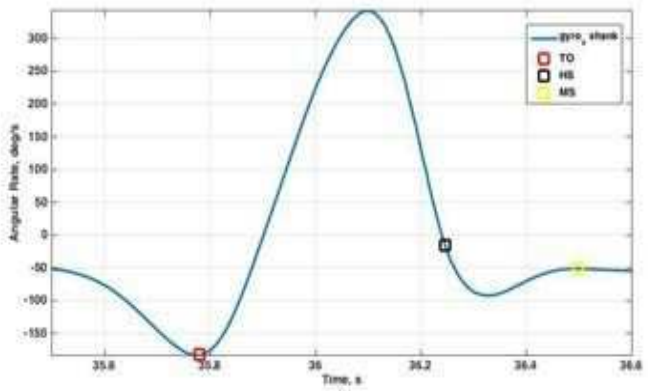

Figure 5.4: An example of gait pattern extracted from gyroscope data for the identification of Toe-off (in red), Heel-strike (in black), and Mid-stance (in yellow) [61].

Looking at Figure 5.4, the reader can lead to three remarks:

- The mid-stance is the point where the flexion-extension of the knee is zero, in other words, the instant marked by absence of rotation.

- The heel-strike represents the moment when the angular velocity crosses the zero and this testifies on the shank fluctuation whose rotation becomes negative when it is completely vertical.

- The toe-off is the moment of change between stance and swing phase and can be detected as the instant when the angular velocity reaches the minimum before increasing its value.

Exploiting these considerations, the algorithm identifies, first, these inflection points (Mid-stance, Heel-strike, and Toe-off), and then the related temporal intervals (swing phase, stance phase and GCT) with the procedure reported down below (Figure 5.5).

First, the maximum peak is reached by identifying the peaks over a fixed threshold and then, turning around, it searches for the first minimum corresponding to the toe-off. This reduces the probability of false toe-off instances.

Second, starting from the position of maximum calculated in the previous step, it searches for the first zero-point that corresponds to heel-strike.

Then, the mid-stance instance is detected as the next minimum that follows the zero-point.

This search is iterated for the entire length of the signal obtaining three different vectors per each temporal instant.

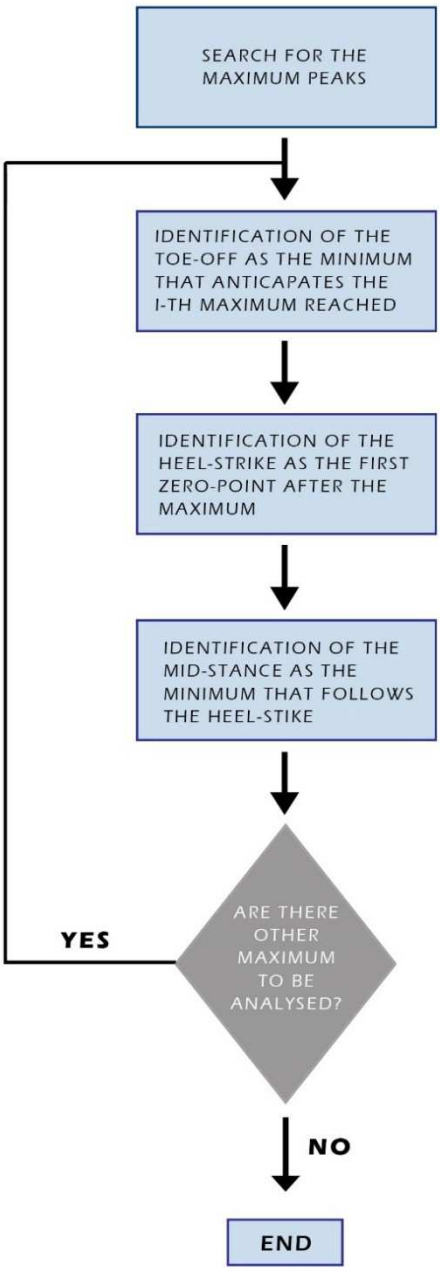

Figure 5.5: Flowchart – temporal instances identification.

Once the temporal instances are available, the GCT is calculated by means of subtractions between consecutive Toe-off instances (TOs) with the expression (5.8).

$$GCT\ (i-1) = TO_{i,\frac{r}{l}} - TO_{i-1,\frac{r}{l}} \qquad i = 1, 2, \ldots\ldots ST \quad (5.8)$$

Where ST is the total number of strides obtained.

The Cadence and Gait Variability are extracted through the inverse of the GCT and considering the ratio between the standard deviation and the mean of the CGT, respectively (see expressions 5.9 and 5.10).

$$Cadence = \frac{1}{GCT} \quad (5.9)$$

$$Gait\ Variability = \frac{1}{100} * \left(\frac{\sigma_{GCT}}{\mu_{GCT}}\right) \quad (5.10)$$

Then, the calculation of Swing and Stance phase is realized (Figure 5.6).

The Swing phase (S_w) is calculated by means of subtractions between Toe-off instance (TO) and the consecutive Heel-strike instance (HS), while, the Stance phase (S_t) is calculated by means of subtractions between Heel-strike instance and the consecutive Toe-off instance as follows:

$$S_w\ (i) = HS_i - TO_i \qquad i = 1, 2, \ldots\ldots ST \quad (5.11)$$

$$S_t\ (i) = TO_{i+1} - HS_i \qquad i = 1, 2, \ldots\ldots ST - 1 \quad (5.12)$$

Consequently, Initial Double Support e Terminal Double Support are calculated through the combination between right and left parameters and then added for obtaining the value of the Double Support (DS) as reported in (5.15).

More specifically, the IDS is calculated as the difference between the left toe-off instances and the right Heel-strike instances (5.13).

Similarly, the TDS is calculated as the difference between the right toe-off instances and the left Heel-strike instances (5.14).

$$IDS = \left(TO_{i,l} - HS_{i,r}\right), \quad i = 1, 2, \ldots\ldots ST \tag{5.13}$$

$$TDS = \left(TO_{i+1,r} - HS_{i,l}\right), \quad i = 1, 2, \ldots\ldots ST \tag{5.14}$$

$$DS = IDS + TDS \tag{5.15}$$

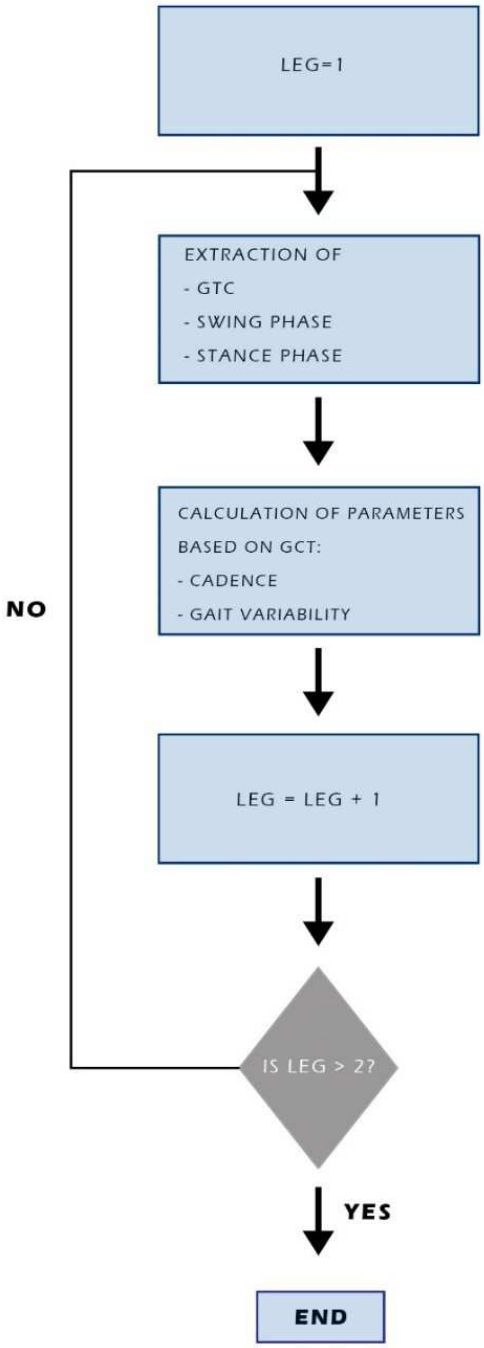

Figure 5.6: Flowchart – temporal intervals identification.

5.3.2 GAIT SPATIAL INTERVALS

The spatial parameters of the gait (e.g. Clearance, Stride Length and Stride speed), are calculated by means of a double integration approach [70].

The gyroscope and accelerometer data extracted from the shank are considered as input to compute both Stride Length and Clearance (whose definitions are exposed in *Chapter 1*).

First, the component of the acceleration along y- and z-axis are converted from the local to the global frame by means of the following rotation matrix:

$$\begin{bmatrix} a_{Y,g}(t) \\ a_{Z,g}(t) \end{bmatrix} = \begin{bmatrix} \cos(\emptyset_{shank}(t)) & -\sin(\emptyset_{shank}(t)) \\ \sin(\emptyset_{shank}(t)) & \cos(\emptyset_{shank}(t)) \end{bmatrix} * \begin{bmatrix} a_y(t) \\ a_z(t) \end{bmatrix} \quad (5.16)$$

Then, $a_{Y,g}(t)$ and $a_{Z,g}(t)$ are updated considering the contribution of the gravity acceleration as follows:

$$\begin{bmatrix} a_{Y,g}(t) \\ a_{Z,g}(t) \end{bmatrix} = \begin{bmatrix} a_{Y,g}(t) \\ a_{Z,g}(t) \end{bmatrix} * g - \begin{bmatrix} 0 \\ g \end{bmatrix} \quad (5.17)$$

Where φ_s is the angle referred to the shank previously extracted, t is referred to every instance between two mid-stance events, and g is the gravity acceleration approximated to 9.81 m/s^2, then subtracted for compensation.

The idea at the base of a double integration approach is to extract the displacement from the acceleration by means of two consecutive integrations as reported in the expressions (5.18) and (5.19).

$$v_Y(MS,i) = \int_{MS,i-1}^{MS,i} a_Y(\tau)d\tau + v_Y(MS,i-1) \qquad i = 1,2, \ldots\ldots ST \qquad (5.18)$$

$$d_Y(MS,i) = \int_{MS,i-1}^{MS,i} v_Y(\tau)d\tau + d_Y(MS,i-1) \qquad i = 1,2, \ldots\ldots ST \qquad (5.19)$$

Where a_Y, v_Y and d_Y are respectively the acceleration, velocity and displacement of the global frame along the Y-axis, and MS is a mid-stance event obtained among the *ST* strides.

Similar is the calculation of both velocity and acceleration on the z-axis.

It may occur that spatial parameters are underestimated, and the two main reasons are:

- The error of the integral drift caused by the specific integration of gyroscope signal;
- The setting of the initial velocity equal to zero at a mid-stance event.

In order to overcome these limits, mostly due to the gap between the ideal consideration and practise, the proposed algorithm acts as follows (Figure 5.7):

- The initial velocity is not approximated to zero, but its value is set as:

$$v_{OS,Y} = \frac{gyr_{s,MS} * l}{100} \qquad (5.20)$$

Where $gyr_{s,MS}$ is the angular rate on the sagittal plane at mid-stance and *l* is the distance between the sensor place on the shank and the ground.

This distance is measured before each data collection.

- The drift is compensated by means of removing a variable quantity, which is decreasing along the advancement of the signal, to both the resulted velocity and displacement (5.21).

$$v_Y(i,ST) = v_Y(i,ST) - v_{OS,Y} * {}^{i}/_{l} \qquad i = 1,2, \ldots\ldots l \qquad (5.21)$$

Where l is the number of samples between two consecutive MS events that varies on each stride (ST).

Then, the Stride Length is calculated considering the whole trajectory made by the inertial sensor on the sagittal plane, while the Clearance can be obtained by considering the maximum displacement obtained on the Z-axis using the following expressions:

$$SL(i) = \sqrt{d_Y(MS,i)^2 + d_z(MS,i)^2} \qquad i = 1,2, \ldots\ldots ST \qquad (5.22)$$

$$Clearance(i) = \max\left(d_{z\,(MS,i-1:\,MS,i)}\right) \qquad i = 1,2, \ldots\ldots ST \qquad (5.23)$$

This stage of the algorithm is concluded with the computation of the speed by simply dividing the stride length by the GCT as follows:

$$\mathrm{SP(i)} = \frac{\mathrm{SL(i)}}{\mathrm{GCT(i)}} \qquad i = 1,2, \ldots\ldots ST \qquad (5.24)$$

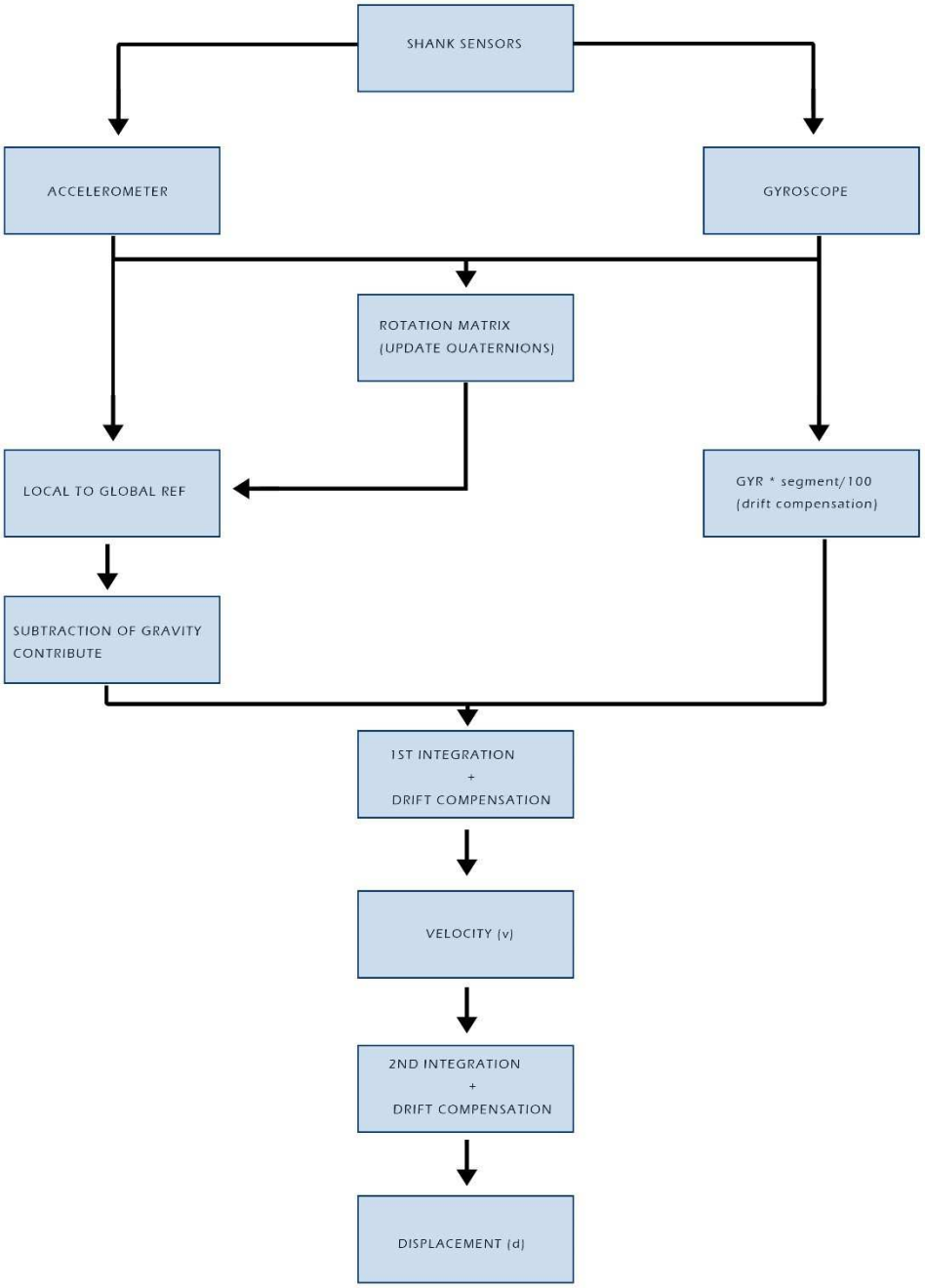

Figure 5.7: Flowchart – Double integration approach to extract the displacement useful for computing the spatial parameter of the gait.

5.4 FEATURES EXTRACTION

To the literature, the feature extraction is generally categorized in three main branches: Time-Domain, Frequency-Domain, and Discrete Domain (Figure 5.8).

The part of the algorithm exposed in the previous paragraphs reflects the common biomechanical approach. In addition to the basic parameters, this stage of the algorithm is focused on taking extra time-domain and frequency-domain features for giving a complete overview of patient's conditions that could be helpful for clinical evaluations [23].

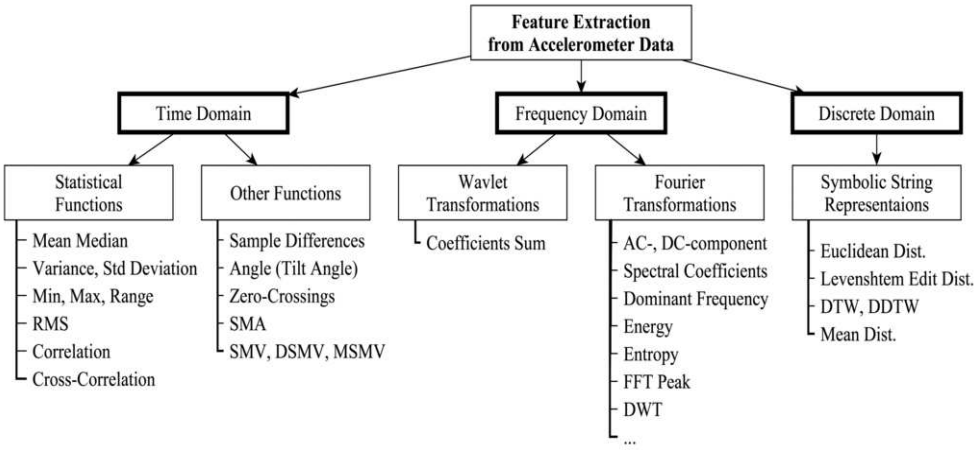

Figure 5.8: Summary of the main features extracted for knee health assessment [71].

The studies that have analysed the patient outcomes in terms of time-domain and frequency-domain features [72-74] showed the usefulness of these variables in defining the signal complexity.

Taking advantage of these results, this study applies most of metrics available in literature to assess changes in motion and motor control in ACLR.

More specifically, the features are extracted per each repetition (or in a shifting window in the case of the entropy-related features) for both legs providing a time-series based model.

The data collected from the unimpaired leg are considered as a reference during the assessment of progress.

Before starting with the the features extraction, the data are segmented through a threshold algorithm to obtain many repetitions, shifting windows in the case of entropy-related features, or strides in the walking sets.

A repetition is obtained by the iteration of the same manoeuvres during an exercise or walking sets, similarly for the stride.

Then, the exercise is cropped in order to select the same number of repetitions/stride per each type of scenario for all data captures.

On the other hand, the moving window is obtained by setting the starting point and considering the next 50% of the signal and shifting the window of the 10% of the signal.

Unlike the common categorization between time-domain and frequency-domain features, this study proposes 7 categories of features:

- gait variables (*see Paragraph 5.3*);
- statistical features;
- kinematic variables;
- info/theoretical, spectral and entropy-related features;
- jerk-based features;
- stability-related features;
- ROM-based features.

In the next subparagraphs an explanation of all the categories and the variables considered for the development of this study is reported.

5.4.1 STATISTICAL VARIABLES

The statistical variables are descriptive time-domain features that give different information about the data set, such as minimum, maximum, or dispersion of the data. These features are extracted from each repetition/stride per each leg.

The variables included in this category are: Minimum, Maximum, Peak-to-peak, Mean, Standard Deviation (Std), Coefficient of Variation (CV), Root mean square (RMS), Skewness, Kurtosis.

Each variable is calculated, first, per each axis, and then, on the magnitude (only in the case of Mean, Std, RMS, Skewness, and Kurtosis) of both accelerometer and gyroscope data to obtain in total a number of 64 statistical parameters.

In Table 5.1 is provided a brief summary of all the variables and their definitions.

Table 5.1: Statistical variable computed in this trial per each session, axis, exercise, segment, repetition/stride.

Variable	Definition
Min	$\min(x_i)$
Max	$\max(x_i)$
Peak-to-peak	$\max(x_i) - \min(x_i)$
Mean (μ)	$\frac{1}{N}\sum_{i=1}^{N} x_i$
Standard Deviation (σ)	$\sqrt{\frac{\sum_{i=1}^{N}(x_i - \mu)^2}{N-1}}$
Coefficient of Variation (CV)	$\frac{\sigma}{\mu}$
Root Mean Square (x_{rms})	$\sqrt{\frac{1}{N}\sum_{i=1}^{N} x_i^2}$
Skewness (γ_1)	$\frac{E(X-\mu)^3}{\sigma^3}$
Kurtosis ($Kurt\,[X]$)	$\frac{E(X-\mu)^4}{\sigma^4}$

5.4.2 KINEMATIC VARIABLES

This category offers an estimation about the kinematics of the movement and involves most of metrics recently used in biomechanical applications.

Before the extraction of the metrics, the raw data are filtered using a 2nd order Butterworth low-pass filter with 3Hz cut-off frequency.

The kinematic variables extracted per each repetition are the following:

- *Range of Angular Velocity (RAV)*

  The angular velocity quantifies the amount of rotation of an object (the knee, in this specific case) per unit of time. The range is intended as the distance between the maximum and minimum value calculated on the magnitude of the angular velocity.

- *Vertical Acceleration*

  The vertical acceleration considers the difference between the gravitational force and magnitude of the acceleration and takes the maximum per each repetition obtaining a vector that characterize the whole exercise.

- *Vertical Velocity*

  The vertical velocity is obtained as the integration of the vertical acceleration over each repetition of the exercise.

- *Fluency*

  Unlike the other metrics, the Fluency is calculated per each axis of the accelerometer data set. It takes the absolute difference on a specific axis between the unfiltered and filtered data and integrates this value over a repetition.

- *Kinetic Value (KV)*

  The Kinetic value is defined in [75] as

$$E = \frac{1}{2} * mv^2 = \frac{1}{2} * m * \left(\int_{t1}^{t2} a \, \mathrm{dt}\right)^2 \quad (5.25)$$

  Where m is the mass of the subject, a indicates the magnitude of the acceleration and t_1 and t_2 are referred to the start and the end of the single repetition.

5.4.3 INFO/THEORETICAL AND ENTROPY-RELATED FEATURES

This category includes most of spectral, entropy-related and information-theoretic features available in literature [72-74].

In order to derive entropy-related features a Fast Fourier Transform (FFT) is performed.

The FFT is a faster method to compute the Discrete Fourier Transform (DFT). Using the radix-2 Cooley-Turkey method, the FFT can be defined as follows:

$$X_k = \sum_{m=0}^{\frac{N}{2}-1} x_{2m} * e^{\frac{2\pi i}{N}(2m)k} + \sum_{m=0}^{\frac{N}{2}-1} x_{2m+1} * e^{\frac{-2\pi i}{N}(2m+1)k} \quad (5.26)$$

The applied method splits the signal *x* in two parts made by *N/2* samples computing only *(N/2) log₂(N)* complex multiplications and *N log₂(N)* complex additions in respect to the high computational load of the DFT.

The variables included in this category are presented down below and are extracted from the raw inertial data of the 4 WIMUs. Each variable is calculated per each axis of the accelerometer and the gyroscope of both legs.

Lempel-Ziv Complexity

Lempel–Ziv Complexity (LZC) is interpreted as harmonic variability parameter and gives information that concerns the complexity and predictability of the signal. The higher its value, the less the predictability is leading to the identification of complex signals.

Many studies [76, 77] applied LZC on biomedical signal, including Electrocardiograms (ECG), electroencephalograms (EEG), and brain activities.

In this study, the LZC is applied on inertial data. Higher values reflect clumsy manoeuvres and are associated with difficulties in performing a specific exercise. Hence, decreasing values are expected during the progression of ACLR programs.

The LZC algorithm transforms the signal into a symbols sequence for simplifying the computation defining a number of thresholds by the following steps:

1. Compare the signal with the defined threshold;
2. Associate an alphabet symbol to each sample of the signal;

3. Divide the whole sequence of symbols in *i* cells (b_i);
4. Compare element per element the symbols in b_i with the symbols in b_{i-1};
5. Iterate step (4) is iterated adding new symbols in b_i until the current sequence of symbol is already presented in previous cells;
6. Compute the LZC as $\frac{k \log_\alpha n}{n}$ where k is the length of the current cell, n is the length of the signal in a single repetition, and α is generally set at 10;
7. Normalize the LZC on a defined number of levels, generally set at 90

$$\frac{LZC}{\log(levels)} \tag{5.27}$$

Frequency-Domain Entropy

The Frequency Domain Entropy (FER) gives information about the power spectral entropy.

Its calculation starts with the calculation of the PSD of the signal, then the extracted PSD is normalized through a division by the total sum, as follows:

$$\hat{P}(\omega_i) = \frac{1}{N} |X(\omega_i)|^2 \tag{5.28}$$

$$p_i = \frac{\hat{P}(\omega_i)}{\sum_i \hat{P}(\omega_i)} \tag{5.29}$$

Where $|X(\omega_i)|$ is the amplitude spectrum of the signal and N is the number of samples.

Finally, the FER is extracted as follow:

$$FER = -\sum_{i=1}^{n} p_i \ln p_i \tag{5.30}$$

5.4.4 SPECTRAL FEATURES

Similar to the entropy-related, the computation of the spectral features starts with the application of the FFT.

These features are calculated on a defined window of the data set. Following what is already reported in *Paragraph 5.4*, this window is shifted for the 50% with 10% overlapping.

In the case of spectral features, it resulted to be more reasonable to avoid the calculation on a single repetition. Short windows, in fact, lead to the repetition of the same values. On the other hand, larger windows can decrease the accuracy of results.

The metrics evaluated in this trial are Peak Frequency and its width (DMW), Spectral Centroids, Power in 1.5-3 Hz (LFP), Power in 5-8 Hz (MFP), First-Second-Third Quartile frequency, Spectral Edge Frequency at 95% (SEF), Ratio High-Low Bands (RHL) and Harmonic ratio (HR) [71-73]

These features are described more in detail down below.

Peak Frequency

The Peak Frequency, also known as Dominant frequency (DF), is the frequency that shows the maximum spectral power. This metric is calculated following the indication of [72] as follows:

$$f_p = \arg max_{f\in[0,f_{max}]} |F_X(f)|^2 \quad (5.31)$$

where $F_X(f)$ is the Fourier transform of the *X* signal.

On the other hand, the Dominant Frequency Peak Width (DMW) is the range of frequencies which includes the values between the peak and the half peak (Figure 5.9).

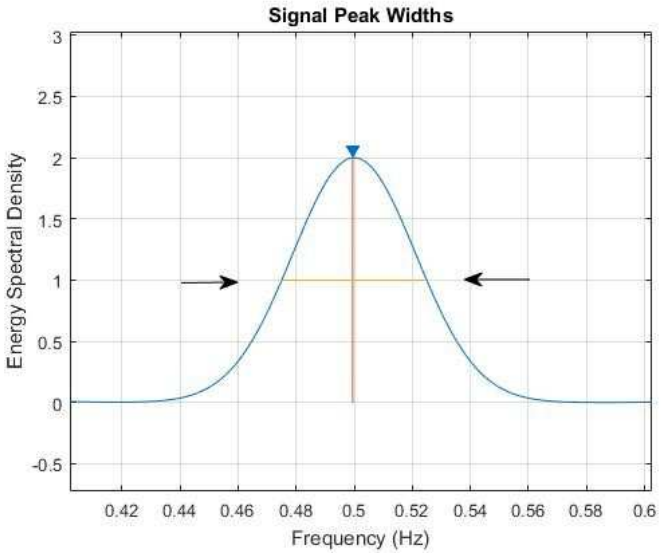

Figure 5.9: An example of calculation of Dominant Frequency and its width. The dominant frequency (triangle) of that window of the signal and the width whose extension (between the arrows) is highlighted by the yellow line.

Spectral Centroids

The spectral centroid (SP) is a metric that gives information about the location of the "center of mass" of the spectrum.

It is calculated per each axis as the weighted mean of the frequencies *f(n)* in the defined shifting window of the signal with their magnitudes *x(n)* as follows:

$$Centroid = \frac{\sum_{n=0}^{N-1} f(n)x(n)}{\sum_{n=0}^{N-1} x(n)} \quad (5.32)$$

Power 1.5-3 Hz / 5-8 Hz

The power spectrum entropy is extracted from acceleration and gyroscope data on a shifting window. It is considered as an alternative metric to the conventional indices of smoothness, such as the jerk measures. [74]

The Power between 1.5 - 3 Hz / 5 -8 Hz (LFP / MFP) are calculated using the expressions (5.33) and (5.34).

$$LFP = \frac{\sum_{1.5-3\ Hz} f}{\sum f} \tag{5.33}$$

$$MFP = \frac{\sum_{5-8\ Hz} f}{\sum f} \tag{5.34}$$

First, Second, And Third Quartile Frequency

The quartile is used in descriptive statistics for dividing a ranked data set in four equal quarters.

The first quartile (25%) and third quartile (75%) considers an interval of the data of the data set and takes the middle number. The interval of the former goes from the smallest number to the median, while the interval of the latter goes from the median and the highest value of the data set. Finally, the second quartile (50%) is identified as the median of data (Figure 5.10).

In this trial, the quartiles are calculated both on the FFT of the signal and on its magnitude per each segmented window.

Spectral Edge Frequency

The Spectral Edge Frequency (SEF) is a common metric used in EEG analysis (Figure 5.11) and it is defined as the frequency below which a defined percentage of the total signal power is located [78]. In this analysis, the defined percentage is set at 95%.

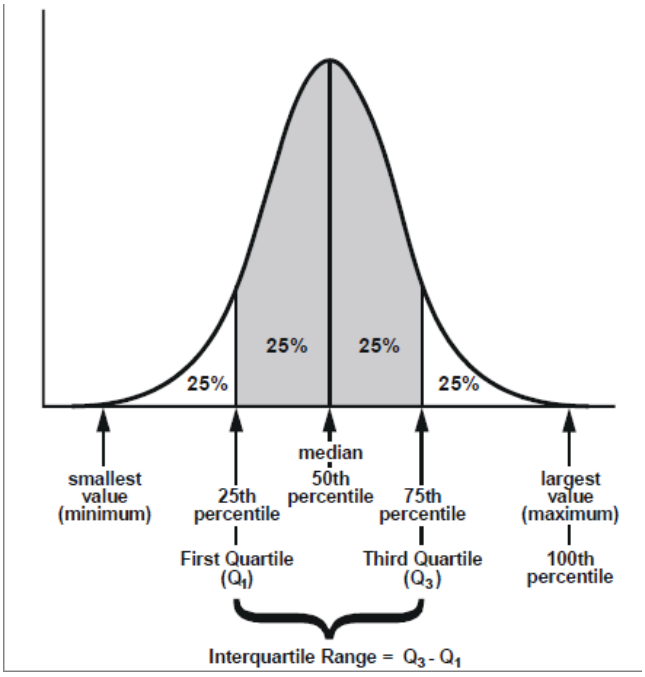

Figure 5.10: A schematic representation of 25%-50%-75% quartiles detection [77].

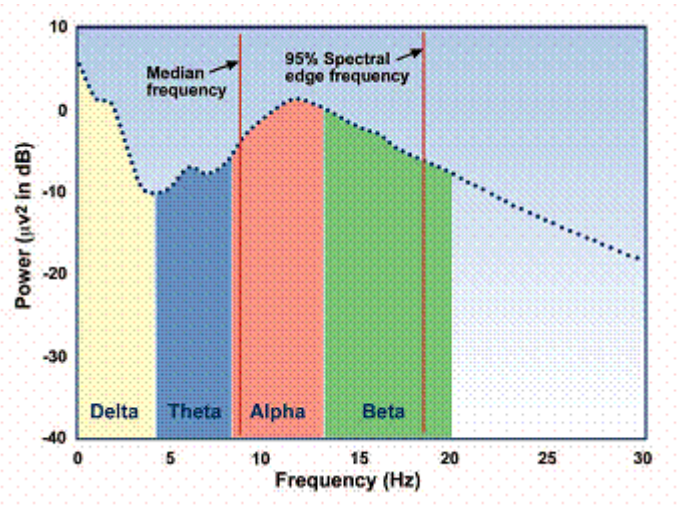

Figure 5.11: An example of SEF calculation in EEG[78].

Ratio High-Low Band

Similar to the calculation of the other spectral features, the Ratio High-Low Band (RHL) starts with the calculation of the FFT and it is defined as:

$$RHL = \frac{\sum_{>5Hz} HF}{\sum_{\leq 5Hz} LF} \quad (5.35)$$

Where HF is the high frequency elements of FFT, and LF is the low frequency FFT elements except for the first element [74].

Harmonic Ratio

The harmonic ratio gives an estimation of the harmonic composition of the accelerometer and gyroscope data [72] for a specific repetition/stride. Its calculation considers the first 20 harmonic coefficients of a shifting window. A greater smoothness of the signal is obtained for higher values of this metric.

5.4.5 JERK BASED FEATURES

The Jerk-based metrics are considered as the conventional metrics used to estimate the smoothness of a signal.

A jerk-based measure depends on the functional $C \int_{t1}^{t2} \dddot{x}(t)^2 dt$, where x is the position, C is the scaling factor, t1 and t2 represents the start and the end of the repetition.

A recent study [79] proved that all jerk-based metrics that quantify smoothness depend on the duration and extension (amplitude) of the movement. An alternative to this dependency is offered by the dimensionless jerk measure.

Most of the jerk-based features available in literature [79] are proposed in this trial. More specifically, each feature is extracted on a single repetition/stride of the exercise for both accelerometer and gyroscope.

The metrics evaluated in this trial are: integrated squared jerk (ISJ), mean squared jerk (MSJ), cumulative square jerk (CSJ), root mean square jerk (RMSJ), mean square jerk normalized by peak speed (N_MSJ), integrated absolute jerk (IAJ), mean absolute jerk normalized by peak speed (N_MAJ), and dimensionless square jerk (DSJ).

These features are defined in [79] as illustrated in Table 5.2.

Except for the DSJ, all metrics strongly decrease when the movement is extended for a longer duration.

For instance, concerning the sensitivity to arrest period and fragmentation, when two sub-movement have no overlapping the values of IJS and N_MSJ remain constant, whereas MSJ and N_MAJ decrease with total movement duration.

The DSJ measure increases monotonically along the change of movement during the exercise, hence it reflects the change of shape along the repetitions of the movement with duration.

Table 5.2: Jerk-based measures computed in this trial per each session, axis, exercise, segment, repetition/stride.

Variable	Definition
Integrated Square Jerk	$\int_{t1}^{t2} \dddot{x}(t)^2 dt$
Mean Squared Jerk	$\frac{1}{t_2 - t_1} \int_{t1}^{t2} \dddot{x}(t)^2 dt$
Cumulative Squared Jerk	$\sum_{k=1}^{n} \dddot{x}(t_k)^2$
Root Mean Squared Jerk	$\sqrt{\frac{1}{t_2 - t_1} \int_{t1}^{t2} \dddot{x}(t)^2 dt}$
Mean Squared Jerk Normalized by peak speed	$\frac{1}{v_{peak}(t_2 - t_1)} \int_{t1}^{t2} \dddot{x}(t)^2 dt$
Integrated Absolute Jerk	$\int_{t1}^{t2} \lvert \dddot{x}(t)^2 \rvert dt$
Mean Absolute Jerk Normalized by peak speed	$\frac{1}{v_{peak}(t_2 - t_1)} \int_{t1}^{t2} \lvert \dddot{x}(t)^2 \rvert dt$
Dimensionless Squared Jerk	$-\frac{(t_2 - t_1)^5}{v^2_{peak}} \int_{t1}^{t2} \left\lvert \frac{d^2 v(t)}{dt^2} \right\rvert^2 dt$

5.4.6 STABILITY

Several metrics have been proposed in literature to quantify the stability, most of them are applied on walking gait performances [75]. Generally, stability indexes are used for prevention of falls or quantitative assessments during rehab procedures. These indexes present high variability when subjects show a great instability during the performance of an exercise or walking gait.

In this specific case, the stability is calculated on the axes of both accelerometer and gyroscope and is extracted by means of the dynamic time warping (DTW) of the signal at two consecutive executions/strides of the exercise as illustrated in 5.36.

$$I_{sta} = \sum_{i=1}^{n-1} DTW \tag{5.36}$$

5.4.7 RANGE OF MOTION

The knee Range of Motion (ROM) offers an idea about the ability in performing a defined movement in a specific plane (Figure 5.12). This metric is the most common metric evaluated in literature that can be measured in both clinical assessment and laboratory environments with different levels of accuracy (see *Chapter 2*).

In this trial, this parameter is extracted per each axis of the accelerometer and gyroscope considering the peak-to-peak amplitude of the signal within a specific repetition/stride.

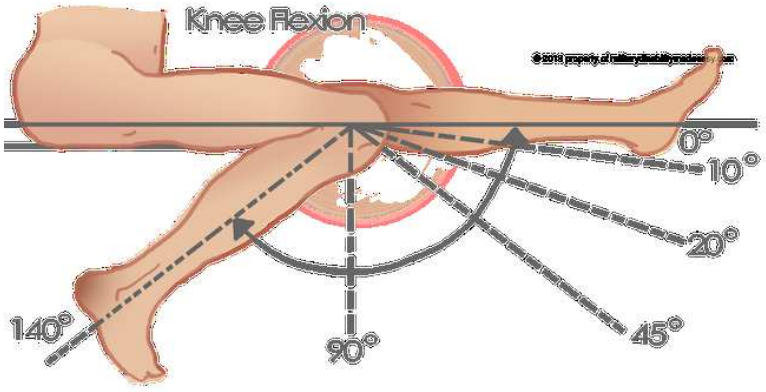

Figure 5.12: Range of Motion (ROM) during knee flexion on the frontal plane [80].

A wide range of features makes challenging the classification of patients' progress due to the intrinsic variability of the parameters. Hence, a features selection algorithm is applied for selecting the most informative features among the ones described above. Then, the selected features are used to calculate the score indicator as exposed in the next Chapter.

CHAPTER 6

Performance evaluation

A classification method is based on characterizing an object or a subject in based on a selected range of features which should be relevant for the considered task.

The classification of an object involves the so-called "machine learning" technique. The machine learning is a subfield of artificial intelligence that is based on creating a system able to solve a problem by training it.

The machine learning techniques can be distinguished between supervised, unsupervised and reinforcement learning (Figure 6.1).

The supervised learning is based on training a classifier through a known data-set (where "known data set" means that the user knows the class of each object). On the other hand, the unsupervised learning techniques are inferring the class of unlabelled data through the definition of functions. Finally, the reinforcement learning is based on updating the current solution by assigning a reward value obtained through the interaction with the environment.

The choice among the several methods generally depends on the number of subjects available during the trial (Figure 6.2).

The possible alternatives are to evaluate:

- *a single subject at one time*

  This is generally applied in the case of action recognition, when a single subject performs different manoeuvres classified with machine learning technique. [27]

- *a single subject at different times*

  This strategy allows the monitoring of the patient along the rehabilitation program and it helps in defining its health status by looking at the progression during weeks.

- *multi subjects using the same or different groups for training and testing*

  When a greater quantity of subject is available is it possible to use classify the impaired subjects using the healthy ones as a reference.

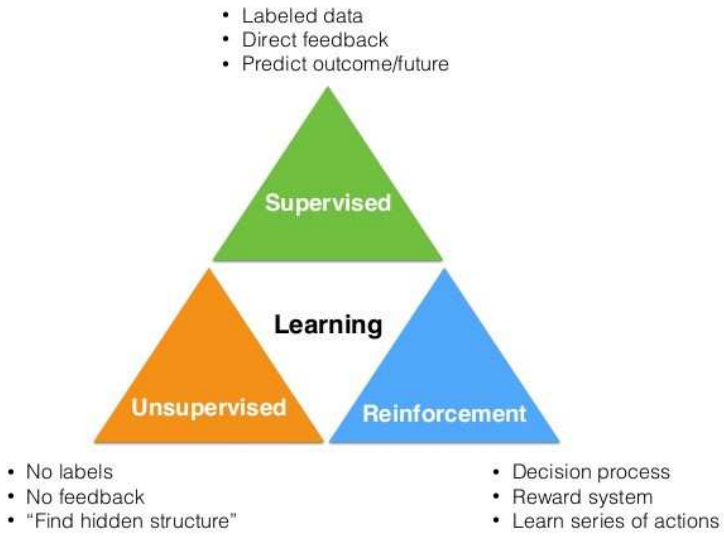

Figure 6.1: Categorization of classification methods [81].

The approach of this trial is inspired by the second and third methods.

It aims, in fact, to classify a single patient at different times looking at the variations in the extracted parameters (see *Chapter 5*).

On the other hand, to monitor the injured limb without a reference could help in defining the improvements of the patient but makes the identification of the health

status challenging. Thus, it is possible to know if the patient is getting better, but it is not possible to identify how far is the patient from the complete recovery.

Another factor that makes the classification challenging is the intrinsic variability of the parameters used to monitor the progresses.

To overcome these limitations, this trial proposes to:

- use the unimpaired leg as a reference, in order to get normative values to which compare the outcomes of the injured leg;
- compute a distance metric that gives as output the difference between the two legs considering all the sources of variability.

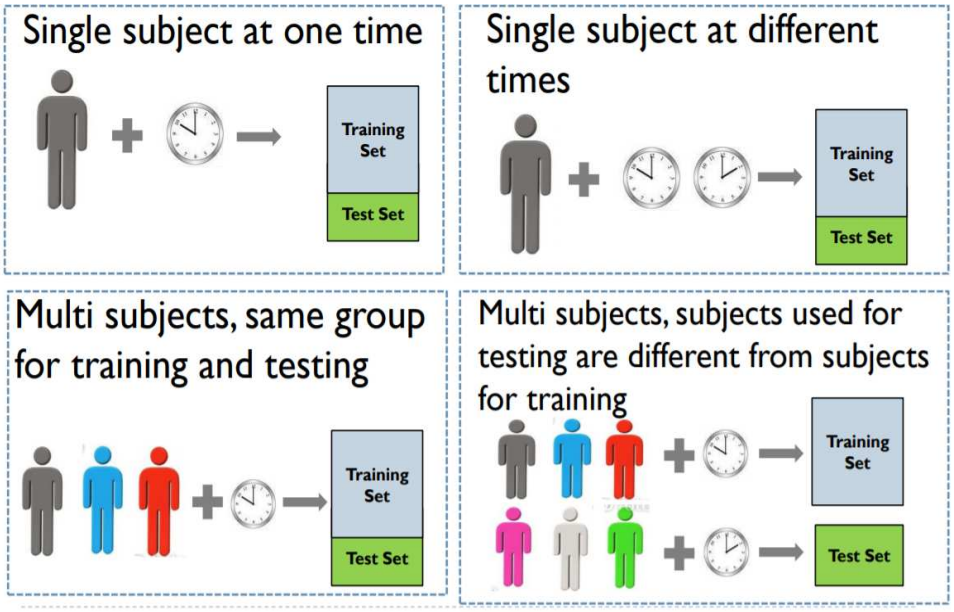

Figure 6.2: Different methods used to classify the patient during rehabilitation [82].

6.1 THE ROLE OF DISTANCE METRICS

A previous analysis confirmed that a single parameter is insufficient for giving an estimation of rehabilitation trends, but their analysis overall lead to comprehensive overview of the patients' health status [23].

Therefore, it is necessary to define a single indicator that involves in its calculation all the extracted features to support the assessment of the patients' performances by clinicians during clinical practice.

To this purpose, different types of distance metrics can be considered.

Distance metrics generally takes into account the distance between two probability distributions for estimating their similarity.

This strategy has been proposed in different studies to quantify both the quality of the performances and the improvement of the subjects. This assessment is generally developed by comparing the manoeuvres performed by a single patient to the average performance obtained by healthy subjects.

To date, two valuable distance metrics founded in literature are the Mahalanobis distance and Bhattacharyya distance [23,55,83-85].

In the next section an explanation of both distance metrics and their application to this trial are reported.

6.1.1. MAHALANOBIS DISTANCE

The Mahalanobis distance (D_M) was first introduced in 1936 and is a statistical measure of the distance between defined point P and distribution D [55, 86].

This distance is mainly based on the correlations between features which help in detecting different pattern that are along a sequence. This determines the similarity of a new data set in respect to a reference.

The problem starts with a fixed set of elements whose class is known and concerns to detect the probability that a defined point P in the n-dimensional Euclidean space

belongs to that set. It is clear that the less is the distance between the point and the center of mass (CoM) of the set, more is the probability of the point to belong to the set.

The simplest approach is to calculate the standard deviation of the samples from the CoM: when the distance between the sample and the CoM is lower than a defined threshold it is likely the belonging of the sample to the current set.

This concept can be expressed with the normalized distance of the sample from the set as $\frac{X - \alpha}{\sigma}$.

This idea of considering only the distance between the sample and the CoM is limited to a spherical distribution of the samples, in fact, when the samples result to have an ellipsoidal distribution also the direction should be taken into account.

Hence, in case of non-spherical distribution of the data set, the covariance matrix of the sample can reflect the probability distribution of the set.

It can be modelled as the distance between the *N-dimensional* feature vector of the patient, $v_P = (v_{P1}, v_{P2}, v_{P3}, \dots v_{Pn})$, in respect to feature vector of the control group $v_H = (v_{H1}, v_{H2}, v_{H3}, \dots v_{Hn})$.

Considering S as the covariance matrix, the D_M can be expressed as:

$$D_M(x) = \sqrt{(v_P - v_H)^T S^{-1} (v_P - v_H)} \quad (6.1)$$

6.1.2 BHATTACHARYYA DISTANCE

The Bhattacharyya distance (D_B) takes the name from its inventor who proposed it in the review: "*On a measure of divergence between two statistical populations defined by their probability distributions*"[87]. It presents different fields of application such as image processing, pattern recognition, machine learning for speaker recognition [83-85].

The D_B helps in identifying the similarity between two data sets by comparing two samples taken from the two distributions.

Unlike the D_M, the D_B is not limited to the analysis of two distributions that present the same standard deviations, in fact, tends to increase its value in proportion to the distance between them (in the same case the D_M resulted to be zero). This consideration makes the D_M a particular case of D_B.

The D_B starts its computation from the Bhattacharyya Coefficient (BC). The BC is an index that quantifies the overlapping between two probability distributions by evaluating the distance between two samples.

The whole distribution is divided in *n* partitions, then, two general elements p_i and q_i of *n-th* partition generate the BC with the expression (6.2).

$$BC(p,q) = \sum_{i=1}^{n} \sqrt{p_i q_i} \tag{6.2}$$

Consequently, the D_B can be calculated as follows:

$$DB(p,q) = -\ln\big(BC(p,q)\big) \tag{6.3}$$

In the case of two classes, which present normal distribution, the calculation of the D_B is based on the calculation of the mean (μ_p, μ_q) and the variances (σ_p^2, σ_q^2) of the two separated classes and can be simplified as follows:

$$\mathrm{D}_B(p,q) = \frac{1}{4}\ln\left(\frac{1}{4}\left(\frac{\sigma_p^2}{\sigma_q^2} + \frac{\sigma_q^2}{\sigma_p^2} + 2\right)\right) + \frac{1}{4}\left(\frac{(\mu_p - \mu_q)^2}{\sigma_p^2 + \sigma_q^2}\right) \tag{6.4}$$

In the case of two statistical distributions that show the same standard deviations the D_B coincides with the D_M.

6.1.3 THE APPLICATION OF BHATTACHARYYA DISTANCE IN ACLR

Looking at the explanation of the previous paragraph, both metrics provides information for supporting the assessment of clinicians during rehabilitation programs. The metrics can measure how far is the quality performance of the subject from the control group.

On the other hand, the D_M is less applicable due to the necessity to have two distributions that present the same standard deviation.

This necessity results to be very restrictive in the case of ACLR due to the difficulty in having similar standard deviations in control and patient group.

For these reasons, this trial proposed the use of D_B as a more reliable extension to the D_M.

In this specific case, the D_B is used to define the degree of membership of the patient group to the control group. More specifically, the degree of membership is quantified by the D_B and gives information about the closeness between the performance of the injured side in respect to the healthy one.

As exposed before, the D_B takes into consideration two generic elements p_i and q_i of *n-th* partition. In this specific case, the *n* partitions are obtained by considering a generic feature (described in *Chapter 6*) in a defined number of repetition/stride/sliding windows per each exercise. Each feature is extracted separately from each body segment (e.g. shank and thigh) of both right and left sides. Then, the D_B is calculated after removing possible outliers.

More specifically, the D_B calculation involves the following steps:

- *The creation of the feature vector*

  The vector is created by using all the extracted features. Each feature is available per each exercise and it was previously segmented in order to obtain a value per each repetition/stride/sliding window. Furthermore, the feature vector is calculated in order to analyse separately the results of healthy/unhealthy side and the two body segments.

  After these considerations the feature vector can be expressed as follows:

$$feature_X(side, body\ segment, exercise, session) = \left[feature_{X,1}, feature_{X,2}, \dots\ feature_{X,N}\right] \quad (6.5)$$

  Where N is the number of repetitions/stride/window that characterizes each exercise.

- *The removal of outliers*

  An outlier is defined as an observation that is extremely different from the other samples of the distribution. In this analysis, outliers are considered as those values which show more than three scaled median absolute deviations away from the median of the distribution.

  The presence of a potential outlier can adversely affect the final outcome due to its influence on the distribution. To limit this influence, when an outlier occurs it is substituted by the average value from the two nearest samples of the distribution not identified as outliers and a new feature vector is obtained.

- *The calculation of the D_B*

  The new feature vectors are finally used to implement the D_B.

  More in details, the averages and standard deviation of the feature vectors related to both legs are calculated and considered as input for calculating the D_B. This process is iterated until the results in terms of D_B are available per each feature, exercise and session.

- *The implementation of the distance vector*

  Finally, the distance vector is created by the values of the D_B taken for all the session. This distance vector is created per each feature and is available per every exercise and body segment, i.e.:

$$C_{feature_X}(body\ segment, exercise) = \left[D_{B,session1}, D_{B,session2}, \dots\ D_{B,session_m}\right] \quad (6.6)$$

  Where m represents the number of sessions.

In general, the distance vector of each feature should reflect the improvement of the patient during rehabilitation. High values, which testify on a considerable difference between unimpaired and impaired leg, are expected in the first sessions of the rehab program and should tend to zero when the complete recovery is assessed. This consideration needs to be carefully pondered on the intrinsic meaning of each feature and the type of exercise.

For instance, considering hamstring curl ROM over the thigh, it is possible to have a more constant trend of the D_B along the ACLR program. Similar consideration can be developed while considering the exercises that are tested in the post-surgery period (e.g. walking sets, squat rotation and single leg wall slide).

Hence, starting from the D_B related to every exercise, every category, and sensor, this trial tested a feature selection method to discard the uninformative and redundant features in order to offer a more comprehensive assessment of the patient's health status during ACLR.

6.2 FEATURE SELECTION METHODS

A feature selection (FS) approach is defined as every technique which is based on selecting a subset of feature for reducing the dimensionality of a specific data set [82].

Unlike the dimensionality reduction approach, the FS does not involve mathematical functions, but preserves the original measurement unit of the original feature space.

More specifically, the new data set will contain the same number of samples but a lower number of features in respect to the original one.

The purpose of this techniques is to:

- Reduce the computational time;
- Identify the relevant features in relation to the clinical problem, so that the uninformative features would not introduce noise in the overall performance evaluation.

In these applications, it is important to carefully ponder the quantity of selected feature for avoiding the oversimplification of the data set and the consequent loss of important information (Figure 6.3).

More in details, the FS approach is an optimization problem based on two main steps:

1. Search the space of possible feature subset;
2. Evaluate the goodness of each subset through an iterative procedure that continues until the optimal subset is reached.

From a geometrical point of view, it is equivalent to re-projecting the feature space into a lower dimensional subspace perpendicular to the removed features. An example of data set characterizes by a two-dimensional feature space is offered in Figure 6.4.

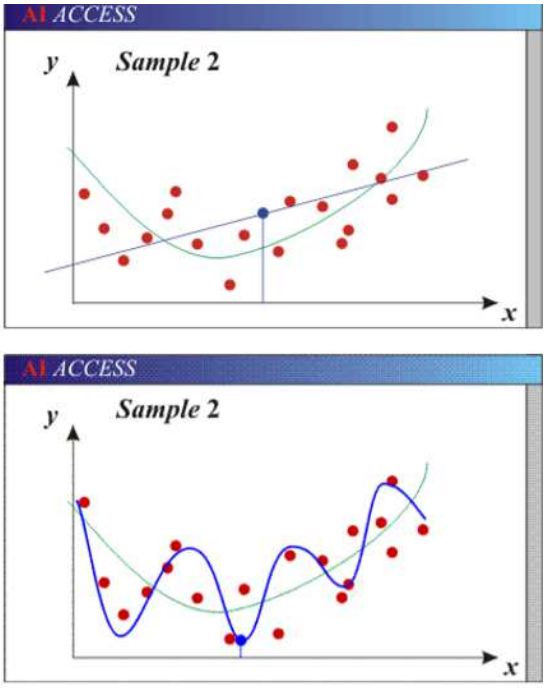

Figure 6.3: On the top, an example of a model with too few parameters that results to be inaccurate due to the large bias. On the bottom, a model with a wide range of parameter whose inaccuracy depends on the large variance [82].

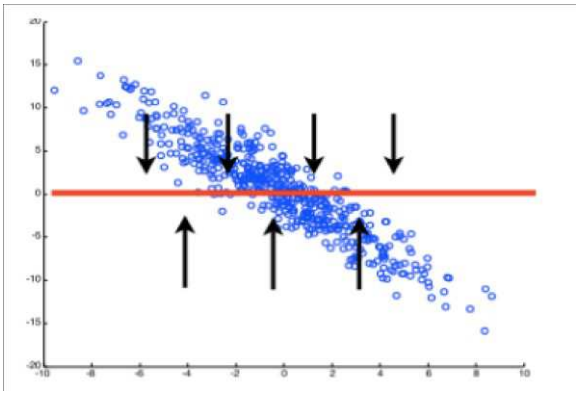

Figure 6.4: Example of data set characterizes by a two-dimensional feature space, then reduced to a lower dimension [82].

The typical applications that involves unsupervised methods are generally based on clustering (Figure 6.5). The instances are partitioned into a number of classes (clusters) based on the both the maximization of similarity of instances inside the same cluster and minimization of similarity of instances of different clusters.

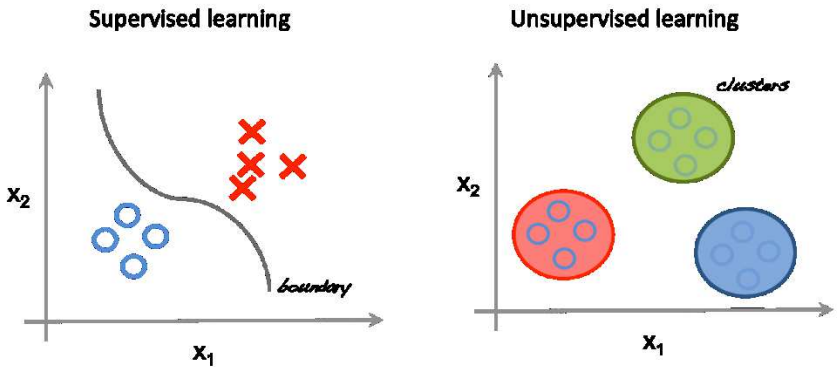

Figure 6.5: Supervised and unsupervised learning clustering method [88].

In this thesis, the aim is to infer the unknown class of data-set without the guidance of a labelled training set, hence, it is necessary to opt for an unsupervised method that is additionally characterized by a low computational load and a good level of accuracy.

To this purpose, in the next subparagraph the description a simple unsupervised method and its specific cases is presented.

6.2.1 K- MEANS CLUSTERING

The simplest unsupervised clustering method that could be founded in literature is the K-means. It mainly consists in classifying each object by computing the Euclidian distance between that object and the centroids of the *K* cluster. The object is assigned to the cluster in which the nearest centroid is placed, and the centroids are initialized randomly. Then, the centroids are recalculated, and the procedure is iterated until no variations are seen in the element assignment. The last step is based on minimizing the objective function.

It should be considered that this approach is well-performed only in the case of very specific assumptions regarding the distribution of the subsets (e.g. only if the distributions has a single mode and very similar variances).

For overcoming these restricted assumptions, an alternative solution is offered by the so-called "weighted K-means". It is also based on a two-phase iterative process in which each element of the data set is assigned to the class of the nearest centroid, but unlike the traditional K-means, fixed weights are assigned to data instances [89]. The two-phase iterative process continues updating the centroids in each iteration using the weights until the optimization of the objective function is reached.

To achieve low computational times and a good level of accuracy, this work applies the new weighted K-means method proposed in [91] for defining the optimal subset of features that allows the description of the progress of patient in each exercise, category, and sensor (e.g. thigh and shank).

This new method is known as Clustering Coefficient of Variation (CVV) and is based on clustering the features in based on their variability (e.g. CV). More in details, it computes the distance between the calculated variance of each feature and the centroid (or the mean).

The CVV proved to be very suitable for classifying biomedical data that present a wide range of features with a low computational load.

6.2.2 WEIGHTED K-MEANS CLUSTERING IN ACLR

In this trial one of the two techniques founded in literature is tested: the Clustering Coefficient of Variation (CCV).

As exposed in the previous paragraph, this technique chooses the optimal clustering according to the CV of the features.

Comparing a wide range of features could be challenging, hence, a method that quantify the dispersion of data is necessary. To this purpose, the CV helps in quantifying the distribution of a data set. More in details, the CV is calculated dividing the standard deviation by the mean of the distribution, and gives, therefore, an estimation about the variability of the data set. This calculation is applied on every m-dimensional vector expressed in (6.6) (e.g. $C_{feature_X}$) .

The higher its value, the more disperses the data.

For selecting the features, the algorithm proposed the procedure proposed in [90] which is reported down below and shown in Figure 6.6:

1. A threshold set on the CV help in selecting a restricted number of feature. Therefore, the algorithm takes into account only the variables that present a CV higher than one, discarding the others.

2. Each distribution is aligned to a normal one in order to avoid any effect of the scaling on the clustering results. More specifically, the remaining variables are normalised using the standard score (e.g. by subtracting the mean and dividing by the standard deviation).

3. At this point the weighted K-means clustering technique is applied to the normalized space of features, where K is fixed at two following the indication of [91]. In each step an element is assigned to the cluster in which the nearest centroid is place. The centroids are initialised randomly. The K-mean technique is iterated 100 times always with different initialization and chooses the cluster that shows the lowest residuals. Both residual and centroids are adjusted by normalizing each variable in respect to the sum of the CV of all the *m* variables.

4. The results of the K-means are used to obtain a scoring vector. In particular, the K-means splits the *m* features in two clusters with number of elements t_1 and t_2, respectively.

5. Per each cluster the average among the *X* variables of the m-dimensional vector is calculated, and the result is normalised between [0,1].

6. Finally, the best subset of feature is chosen following the Hyper-Pipes concept. The Hyper-Pipes concept is based on taking into account the minimum and maximum of each selected feature in the m-dimensional vector, defining a set of ranges. Each range is compared to the one calculated on the average and the best outcome is given by the cluster that offers the highest number of matches.

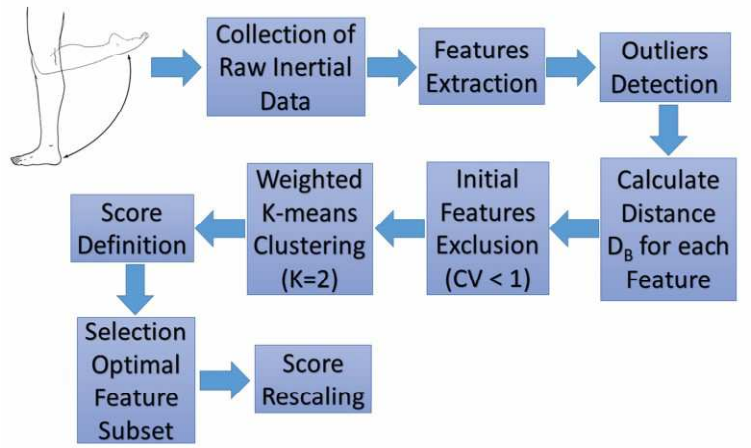

Figure 6.6 Computation of the score indicator [90].

CHAPTER 7

Results and Discussion

Starting from the features described in *Chapter 5*, the performances of the patient are evaluated using the score indicator based on the CVV that was presented in *Chapter 6.* More specifically, the score indicator is computed per each category, body segment, exercise, and session, resulting in a trend.
The results of score indicator relative to each category and exercise are reported in the next sections, then a discussion of the outcome, conclusion and future developments are undertaken.

7.1 RESULTS

The results of the score indicator related to each of the 7 categories of features are proposed in order as follows:

- gait variables;
- kinematic variables;
- ROM-based features;
- stability-related features;
- statistical features;
- jerk-based features;
- info/theoretical, spectral and entropy-related features.

7.1.1 GAIT VARIABLES

The score of the walking sets shows a constant trend with few isolated peaks. The highest values are focused on the 5th session for both walking at 3 and 4 km/h, while on the 1st session for walking at 6 km/h.

The number of features selected are 2, 2 and 3 for walking at 3,4 and 6 km/h, respectively. More specifically, the selected features vary on type of walking set (e.g. GCT and Swing Phase for walking at 3km/h, Stance phase and Clearance for walking at 4 km/h, GCT, Stride Length and Stride Speed for walking at 6 km/h). The discussed results are shown in Figure 7.1.

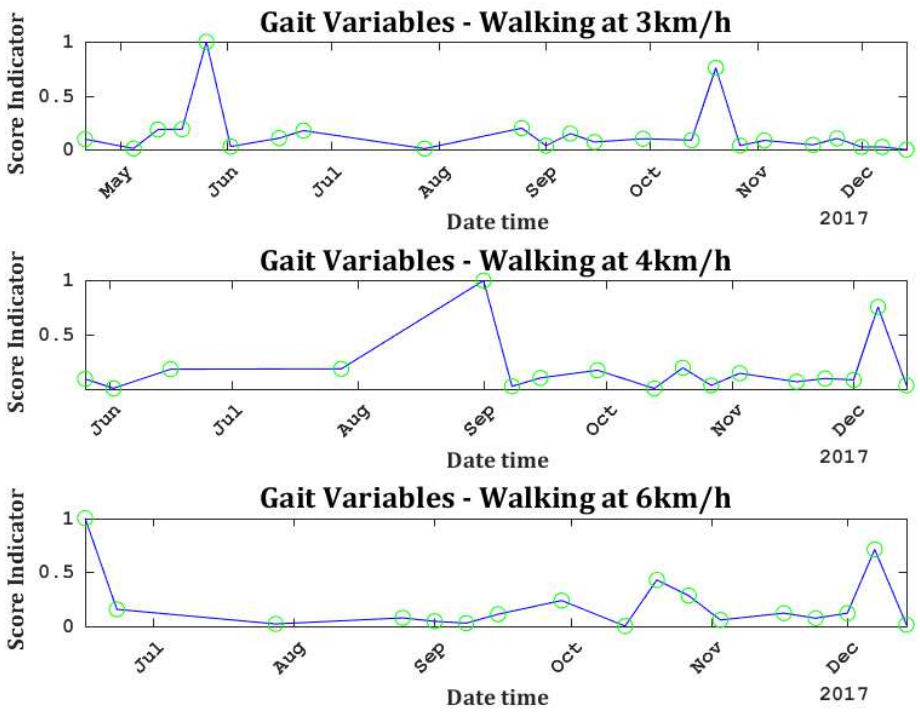

Figure 7.1: Score Indicator relative to the Gait variables for the walking sets. The value obtained per each session highlighted by the green circle.

7.1.2 KINEMATIC VARIABLES

In the *hamstring curl* scenario, the score given by the selected features (e.g. RAV, VV and KV) obtained for the shank sensor shows a trend that presents its maximum peak immediately after the surgery and decreases in the long-term view, even if the last two sessions are characterized by higher values in respect to the previous weeks probably due to the application of mental distractions.

A similar trend is shown for the thigh sensor in which the selected features are (RAV, x-, y- and z-Fluency). In this case an increasing of the score is detected in the post-surgery for reaching the worst condition in the 2th session. Higher values are also shown in the last phase of the rehab program, even if in this scenario it should be taken into account that the thigh has less influence in performing the movement in respect to the thigh, for this reason its consideration should be carefully pondered.

In performing *flexion-extension*, the trend of the shank sensor shows the largest score value given by the selected features (e.g. VA, Fluency over x- and z-axis and KV) in the 2nd session according to the surgery, then the rehabilitation follows a not monotonic response. The score values of thigh sensor determined only by RAV results to be higher around the 3th and 6th sessions.

The *squat rotation* scenario is evaluated only in the post-surgery period following the standards of rehab programs. Evaluating the score based on one selected feature (e.g. RAV) obtained from the shank, no decreasing trends are detected. The largest value of the score is obtained in the 5th session. On the other hand, considering the VA and Fluency over the y-axis selected from the thigh sensor, a decreasing trend is obtained throughout the available sessions.

The *walking gait at 3km/h* for the shank sensor shows reduced values of the score, determined by the single RAV, immediately after the surgery. Similarly, the RAV is also selected for the thigh in addition to VV, and Fluency over x-axis and z-axis.

Increasing speed (e.g. *walking gait at 4 km/h*) lead to a less marked trend, with isolated peaks in which the score is determined by VV, and Fluency over the y-axis in the case of the shank, RAV and KV in the case of the thigh.

Finally, *walking at 6km/h* shows a jagged trend given by the chosen Fluency over x-, y- and z- axis. On the other hand, observing the score extracted for the thigh, the trend results to be smoother in respect to the shank sensor and is obtained with the selected RAV, VA, VV and KV.

It should be taken into consideration that only the period that follows the surgery is analysed, hence, no important improvements could be seen in this phase.

The score indicators that show a clearer decreasing trend are shown in Figure 7.2.

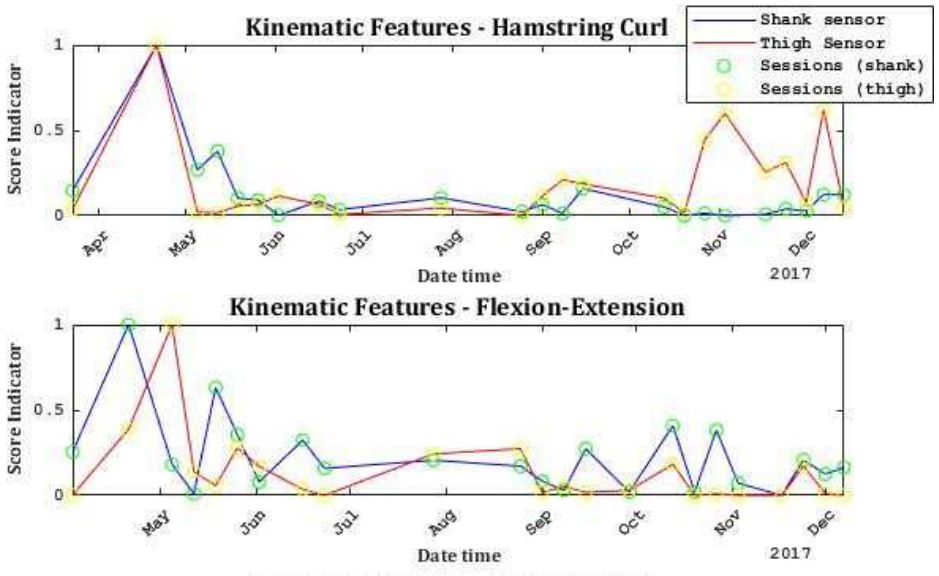

Figure 7.2 Score Indicator relative to the Kinematic Features for hamstring curl, flexion-extension scenarios. The value obtained per each session is highlighted by the yellow and green circles.

7.1.3 ROM-RELATED FEATURES

The selected features for the *hamstring curl* reveal to be ROM over x- and y-axis. The trend is clearly decreasing with high scores more focused in the post-surgery phase.

Regarding the trend during the *flexion-extension* scenario a similar explanation can be given after the selection of the ROM over the y-axis. It can be advertised a clear improvement in both hamstring curl and flexion-extension after the 5th session despite the presence of larger values of the score around 19th session.

Concerning the *squat rotation*, the score is determined by the ROM over the x-axis and shows a decline of the values throughout the session, even if the trend is not monotonic. A clear peak is showed in the 4th session, which can be explained by the swelling and squeaking which affected the patient around that session.

The ROM over the x-axis is also selected for defining the score of the *walking session at 6km/h*. In this case no decline of the score is detected with scattered peaks around the 2nd, 4th, and 13th and 16th. No evident values of the score mark the first part of the plot, which seems to be coherent considering that the change pre-to-post surgery is not available for walking sets.

Similar trends are shown for *walking at 3 and 4 km/h* by selecting ROM over y- and z- axis. Following these explanations, the patient is not following a clear improvement in the last phase of rehab.

7.1.4 STABILITY-RELATED VARIABLES

Concerning the *hamstring curl* scenario, the selected features are stability over x-axis for the shank sensor, and stability over y- and z-axis for the thigh sensor. Both

trends show increasing values until the 3nd session, then, a not monotonic improvement characterizes the rehab period after the 5th session.

Similar considerations are developed for the *flexion-extension* scenario for the thigh sensor, which shows a score based on stability over y-axis that is reduced along the sessions, with high values at the beginning of the rehab program (e.g. 2nd and 5th sessions) and in the last session (e.g. 24th session). In the last case, the largest value at the end is explained by the application of mental distractions that could influence the stability. Clearer is the trend obtained for the shank sensor which selected stability over the Z-axis.

Regarding the *squat rotation* scenario, the features selected are stability over z-axis and x-axis for the shank and thigh sensors, respectively. The trend is decreasing along the sessions of the shank sensor with higher values at the beginning. On the other hand, the score of the thigh sensor showed no correlation with the results on the shank, but still shows a high score on the 5th session like the kinematic score which could testify on patient's swelling.

The trend of the score indicator that characterize the scenario descripted above is shown in Figure 7.3.

The *walking sets at 3 and 4 km/h* taken from the shank sensor provides a score based on the stability over y-axis, while, for *walking at 6km/h* the selected axes are x- and y-. The trend shows changings between high and low values throughout the other session with no particular indication of improvements. Similar considerations can be drawn for the thigh sensor which selects the stability over y-axis and z-axis for walking at 3km/h and x- and z-axis for walking at 4 and 6 km/h, respectively.

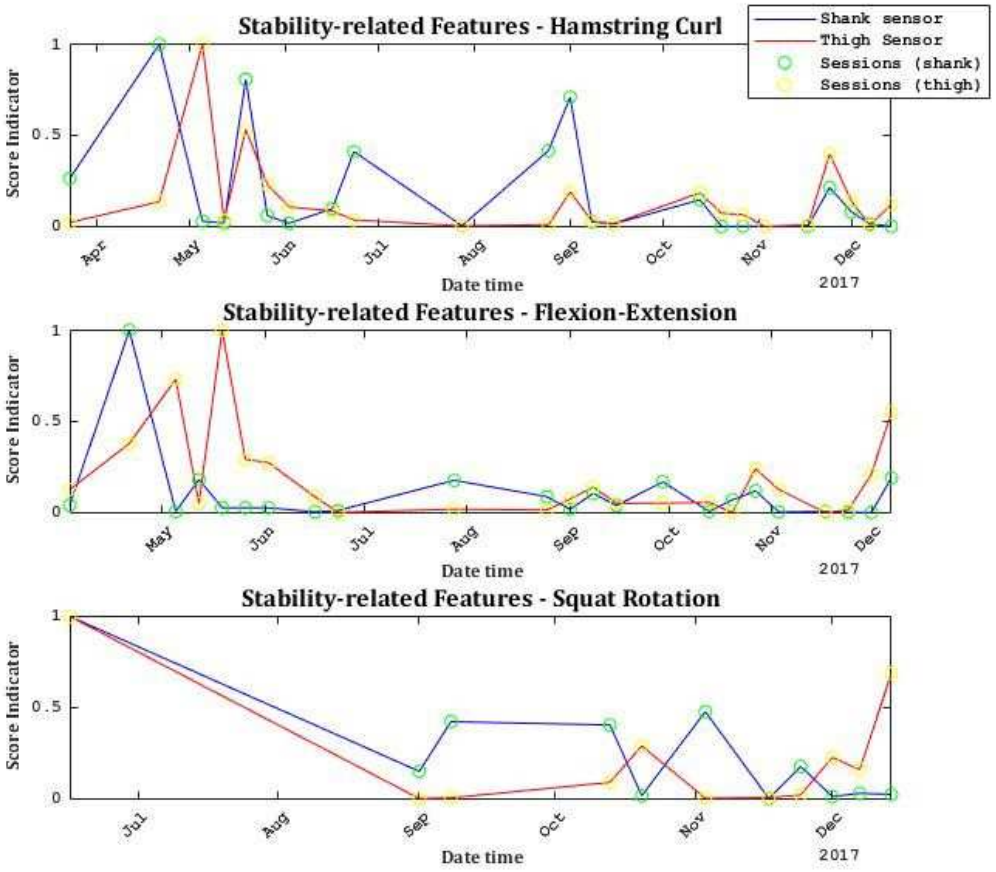

Figure 7.3: Score Indicator relative to the Stability-related features for Hamstring curl, Flexion-extension and Squat rotation scenarios. The value obtained per each session is highlighted by the yellow and green circles.

7.1.5 STATISTICAL FEATURES

In the *hamstring curl* scenario, the score taken from the shank and thigh sensor is based on 20 selected features in both cases. In the former, it shows a score that is reducing its values along the sessions, while, in the latter, no trends can be detected. This tendency is acceptable considering the way the exercise is performed (e.g. the thigh should not be in movement) and thus, it is not particularly interesting in this case for the evaluation of the performances.

The *flexion-extension* scenario shows a number of selected features equal to 17 and 24 in the case of shank and thigh sensor, respectively. Similar to the results obtained for the other categories, the results of both sensors show a score that not monotonically lowers with the advancement of the sessions.

The score relative to the shank and thigh sensors in the case of *squat rotation* scenario is described by 14 and 17 features, respectively, and reveals high values in correspondence to 5th session, which supports the theory of the swelling developed in the categories explained previously. A decline is more marked for the thigh sensor, while, it is harder to assess an improvement along the sessions extracted from the shank sensor.

Regarding the *walking sets at 6 km/h*, both shank and thigh sensor in the statistical score do not reveal any improvement of the patient after selecting 13 and 16 features, respectively. An alternation between high and low values characterized the whole jagged trend. Similar considerations about the trend can be reported for *walking at 3km/h* after choosing 12 and 15 features for shank and thigh, respectively.

On the other hand, a decline of the score is detected in the case of *walking at 4km/h* by selecting 15 features in both shank and thigh.

7.1.6 JERK-BASED FEATURES

In the *hamstring curl* scenario the reduction of the score after the surgery is evident in the results of both shank and thigh sensors. In both cases the decreasing trend is characterized by isolated regressions of the patient. The features selected for the shank on the x-axis are ISJ, MSJ, CSJ, RMSJ, IAJ, and dimensionless jerk, on the y-axis only IAJ, on the z-axis CSJ, RMSJ, IAJ, N_MSJ, N_MAJ, and dimensionless jerk are chosen. On the other hand, for the thigh are chosen on the z-axis are ISJ, MSJ and CSJ, RMSJ and IAJ, while, on the y-axis N_MSJ N_MAJ.

Similar results are obtained the thigh sensor while performing *flexion-extension*. On the other hand, the shank sensor shows increasing values around the 8th session. The features selected for the shank are the same with the only exception of selecting dimensionless jerk instead of IAJ over y-axis. While, for the thigh most of the features are extracted from the x-axis (e.g. ISJ, MSJ, CSJ, RMSJ, N_MSJ, IAJ, N_MAJ and dimensionless jerk), and only one on the z-axis (e.g. dimensionless jerk).

Unlike the previous scenarios, the *squat rotation* showed a reduced number of selected features: only dimensionless jerk over x-axis for the shank sensor, and 8 features for the thigh sensor (e.g. ISJ, MSJ, N_MSJ, N_MAJ on the x-axis, IAJ, N_MAJ, and dimensionless jerk on the y-axis). Concerning the trend, the score of both sensors reveals a not-monotonic improvement.

Walking at 6 km/h shows higher values of the score in the first half of the tested period and reduced values at end of rehab by selecting for the shank sensor 5,1 and 6 features on the x-, y-, and z- axis, respectively. In the case of the thigh only 7 features on the z-axis are chosen.

On the other hand, an improvement can be seen be seen for *walking at 3 km/h* in the results of both shank and thigh, and only in the shank for *walking at 4 km/h*. For the shank sensors 5 (for walking at 3km/h) and 12 (for walking at 4km/h) features are chosen. In the same order, the thigh needs 2 and 13 features.

All promising results that characterize these scenarios are shown in Figure 7.4 and Figure 7.5.

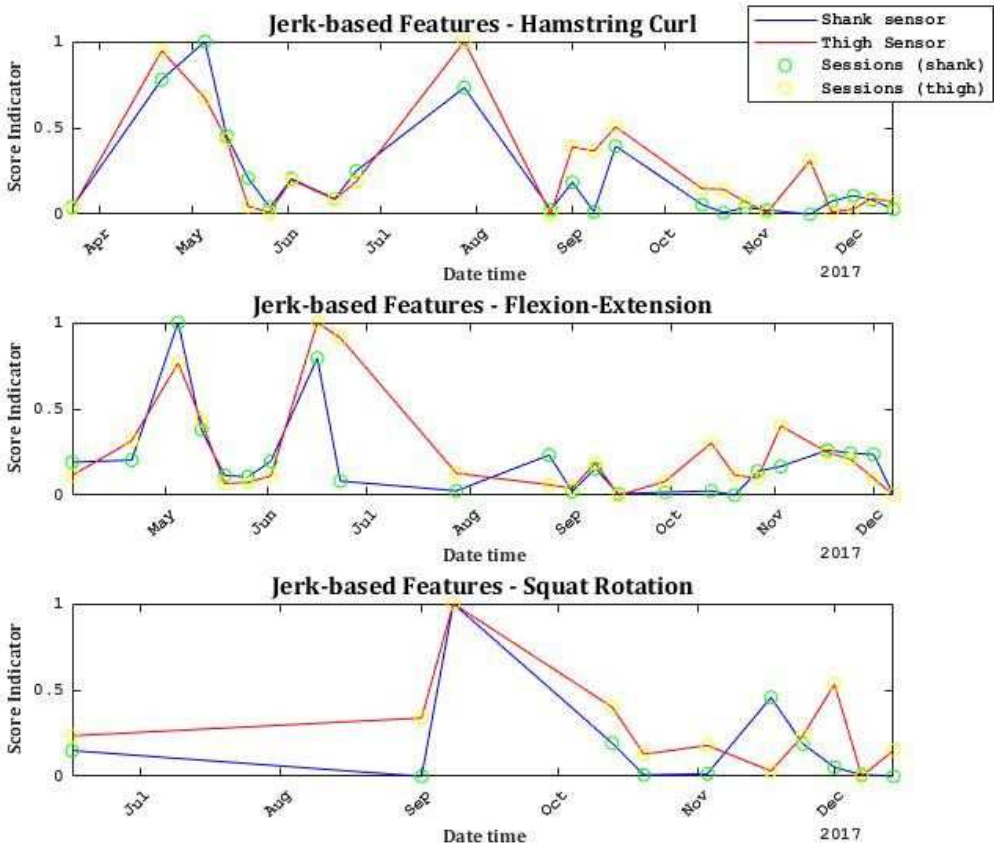

Figure 7.4: Score Indicator relative to the Jerk-based Features for Hamstring Curl, Flexion-extension and Squat rotation. The value obtained per each session is highlighted by the yellow and green circles.

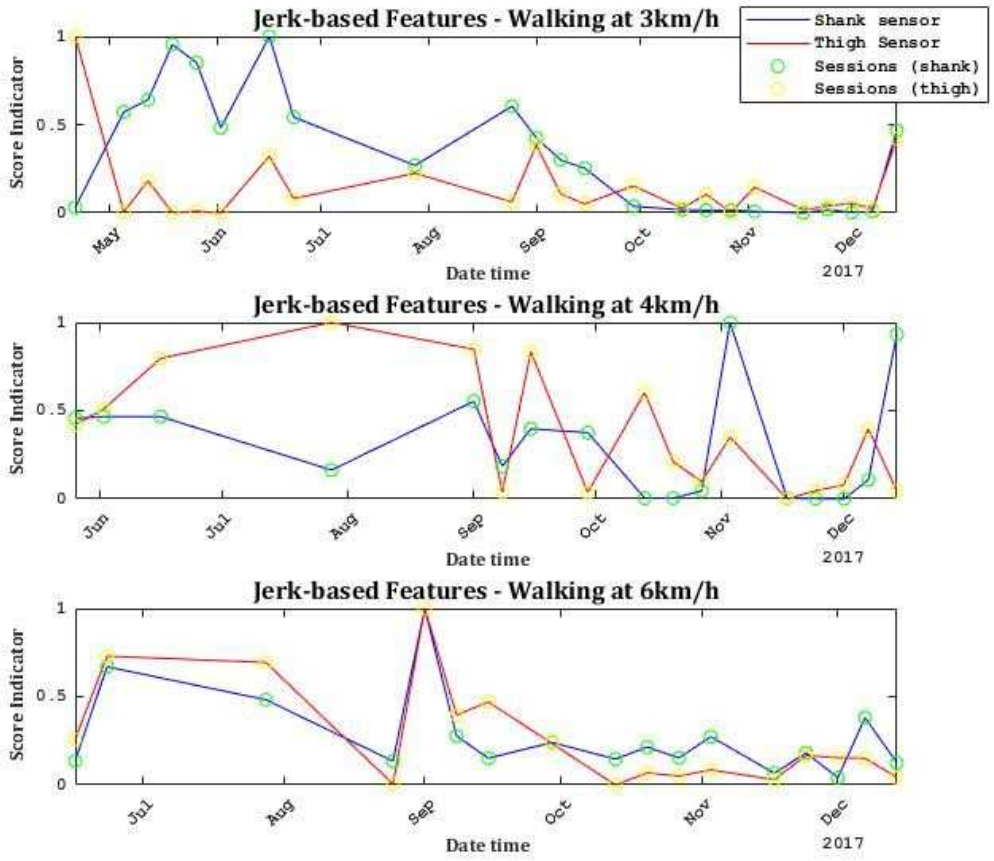

Figure 7.5: Score Indicator relative to the Jerk-based Features for walking at 3, 4, and 6 km/h. The value obtained per each session is highlighted by the yellow and green circles.

7.1.7 INFO/THEORETICAL , SPECTRAL AND ENTROPY-RELATED FEATURES

Concerning the score extracted from the *hamstring curl* scenario, the trend is given by 27 and 29 features for shank and thigh, respectively. In the case of the shank sensor, it decreases until the 10th session, while regressions of the patient can be detected in the 14th and 20th sessions. A clearer improvement is detected for the thigh. The hamstring curl shows both features related to the accelerometer data (e.g. on the x-axis LZC RHL, 3rd Quartile, DMW, on the y-axis LZC, RHL,DF, SC PL

band, PH band, 2nd and 3rd Quartile DMW, on the z-axis LZC, FER, PH band, 3rd quartile, and SEF on the magnitude) and gyroscope data (e.g. on x-axis LZC and DMW, on y-axis LZC,DF and DMW, on z-axis LZC,SC, PH band, DMW and HR).

The score that characterize the *flexion-extension* scenario reflects the same trend detected in the hamstring curl. This trend is determined by the selection of 22 and 27 features for shank and thigh, respectively.

Regarding the *squat rotation* scenario the score selected a lower number of features (e.g. 22 features for the shank sensor, and 23 features for the thigh sensor) related only to the gyroscope data (e.g. LZC over y- and z-axis, FER over z-axis, SC over y- and z-axis, PL and PH bands over y- and z- axis, 1st Quartile on z-axis, 3rd Quartile on x-axis, DMW on y- and z-axis and HR over all the three axis). Higher values of the score are detected around the 6th and 7th sessions, while, the other sessions define a quite constant trend.

Performing the *walking gait at 3 km/h* the score for the shank sensor does not show a clear reduction of the score, the highest values are dispersed along the sessions with high score values placed on the 6th and 12th sessions. The results for the thigh, based on 23 features seems to be correlated with the trend of the shank which is determined by 22 features related to both accelerometer and gyroscope (e.g. SC, LP band, HP band, 2nd and 3rd Quartiles, SEF, DMW and HR from the accelerometer, as well as the gyroscope features with the only exception in taking the LZC on y-axis instead of the 3rd quartile).

Very similar explanations can be reported in the case of *walking sets at 4km/h and 6km/h*. Both sets are described by 27 features in the case of the shank sensor, while 18 and 34 features are necessary for the thigh sensors.

7.2 MUSCLE CONTROL IN SINGLE LEG WALL SLIDE

A different evaluation is undertaken on the Single Leg Wall Slide (SLWS) scenario. This exercise is performed by standing on one leg in squat position while the other leg is lifted, hence, if the patient has not enough strength in the quadriceps he is likely to get into varus-valgus movements. Thus, the more is the shaking of the knee on the medio-lateral axis, the less is the muscle strength of the standing leg.

This work proposed a method to detect irregulates and define the pattern of thigh movement during the performance of SLWL inspired by [92]. This method helps in estimating the muscle control of the patient and the eventual improvements.

It is based on a phase plot-like representation in which the angular velocity measured on the medio-lateral axis is plotted versus the magnitude of the acceleration.

As a result, the straighter the line identified by the distribution, the less the tremor of the leg, leading to a higher muscle control. Vice versa, a more dispersed distribution is synonymous of irregular patterns.

This representation is plotted per each session in which the SLWS is tested and per each leg.

The next stage is to quantify the differences of the distribution between right and left leg along the sessions. In [92] is proposed a quantification based on the "box-counting method" after calculating the fractal dimension.

This work proposed a quantification to avoid the high-computational load typical of the "box-counting method" that results to be accurate enough.

This quantification is based on a circle fitting and follows the steps exposed down below:

1. The y-axis is rescaled in respect to the x-axis in order to get into a circular distribution instead of a unilateral one.
2. The coordinates of the center of circle are set as the mean of the values on both horizontal and vertical axis.

3. The threshold is fixed equal to the 95% of the elements of the distribution.
4. The radius is increased until the number of elements inside the circle are over the threshold. A bigger radius testifies on a more dispersed distribution.

The results obtained after the application of this method are illustrated in Figures 7.6 - 7.13 with a comparison between legs shown in Figure 7.14.

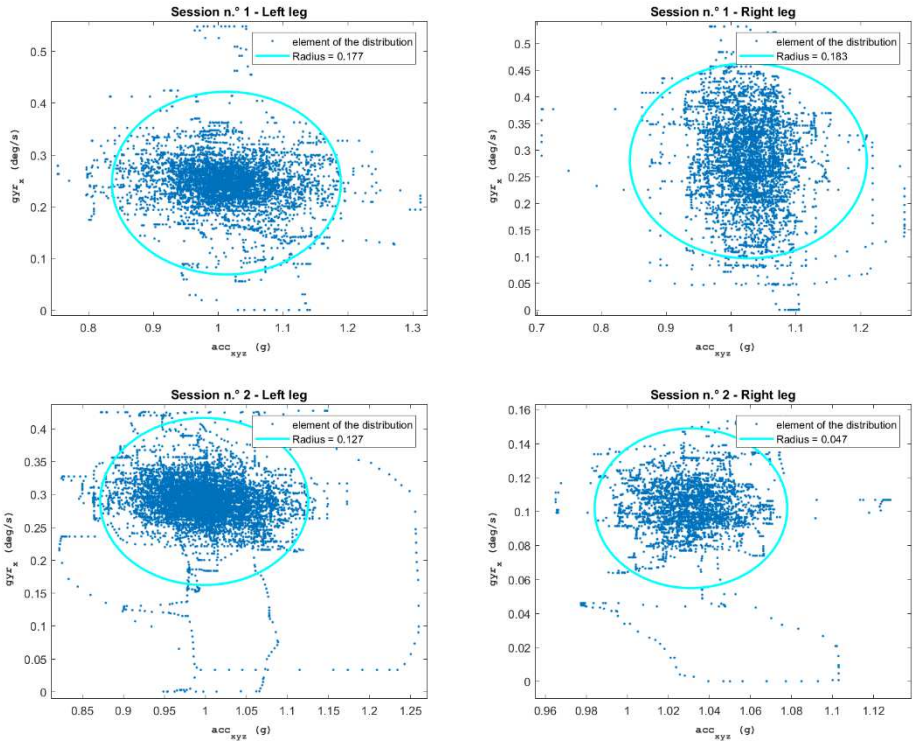

Figures 7.6 - 7.9: SWLS standing on the left leg (on the right) and on the right leg (on the left) during the 1st and 2nd session. The yellow points define the distribution and the cyan circle identifies the maximum extension of the radius in order to include the 95% of the elements.

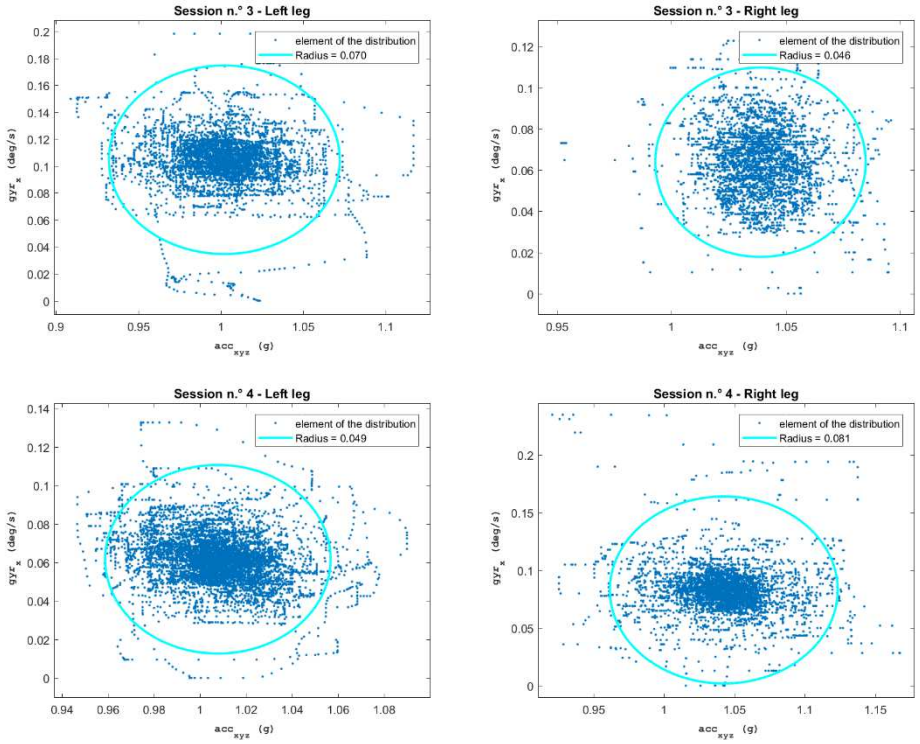

Figures 7.10 - 7.13: SWLS standing on the left leg (on the right) and on the right leg (on the left) during the 3rd and 4th sessions. The yellow points define the distribution and the cyan circle identifies the maximum extension of the radius in order to include the 95% of the elements.

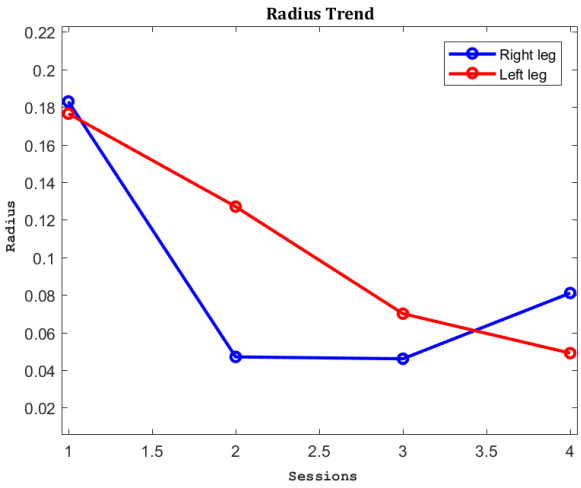

Figures 7.14: Changing in the dimension of the radius among the 4 sessions (Right leg – in blue, Left leg – in red).

7.3 DISCUSSION

This thesis proposes a method for supporting the clinical analysis in defining the knee health status of a patient affected by ACL. The knee is considered the most stressed joint of the lower limbs, thus, it is very likely that it could be injured during sport performances. Considering the increasing number of injuries, systems that enables both short-term and long-term monitoring are required. To date, the gold-standard is represented by clinimetrics and lab-based systems. Unfortunately, none of these systems show all the standard characteristics that a long-term monitoring device should include: practicability, high accuracy, and low-cost. To this purpose, IMUs revealed to be less expensive, more practical, accurate, and easy-to-integrate into a wearable device, and represent, therefore, a suitable solution to be applied in ACLR.

This study testes 4 WIMU developed and validated at Tyndall National Institute for extracting a wide range of parameters and defining the most informative ones through a feature selection method.

The 4 WIMU are used for capturing the data weekly from a young patient affected by ACL. The patient was asked to wear the IMUs by means of stretchable velcro straps and to perform different scenarios (e.g. Hamstring Curl, Flexion-extension, Squat Rotation and walking gait at different speeds).

The algorithm stars with the calculation of the 3D knee joint angles through a quaternion-based fusion algorithm taking into account both accelerometer and gyroscope data.

Then, different categories of parameters are implemented: gait variables, statistical features, kinematic variables, info/theoretical and entropy-related features, jerk-based features, stability-related features and ROM-based features.

Each feature is evaluated in every session, scenario, category, repetition/stride/window, segment and axis (where possible), per both legs. The overall number of computed features per each segment is 181. The number of features per each category is 6, 64, 7, 74, 24, 3, and 3 for gait, statistical, kinematic,

info-theoretical/spectral, jerk-based, stability-related and ROM-based categories, respectively.

The differences between the two legs are estimated in both shank and thigh sensor by using the Bhattacharyya distance (D_B). The expected trend should reveal high values of the D_B immediately after the surgery reducing them throughout the rehab program. It should be also taken into account that many scenarios (e.g. squat rotation and walking sets) are not available in the pre-surgery phase, hence, their trend could be flatter. In order to avoid redundant or uninformative features, the Clustering Coefficient of Variation (CCV) is applied for selecting a subset of features.

The outcome of the CVV is a score which reveals per each exercise and category the optimal subset of features for detecting the patient's improvements.

The gait variables are the most suitable for detecting an improvement related to walking gait performances, even if the type of feature selected varies on the different sets (e.g. at different walking speeds).

The selected kinematic features well-describe the decreasing trend in all exercises, with the only exception of squat rotation and walking at 4 km/h which show isolated high scores along the sessions. This is due to a relative improvement of the patient performances. The most selected features among all exercises are RAV, Fluency over y-axis and KV.

Concerning the ROM-based features, reducing values of the score are detected throughout the sessions of hamstring curl, flexion-extension and squat rotation scenarios. The selected ROM is over the x- and y-axis, only walking at 3 and 4 km/h based their trend on z-axis. Hence, the ROM that defines internal-external variations is not considered meaningful for an ACL assessment that includes the proposed scenarios.

Similar to the consideration developed for the ROM, the stability-related score gives information about the patient's progressions in all exercises, except for walking at 3 and 4 km/h. Considering all the exercises, the stability is selected over all the axis at least one time. For instance, the hamstring curl score chooses the

features along x- and z- axis, while, the flexion-extension score needs only the values along the y- axis.

Then, the statistical score gives poor results revealing that a decreasing trend could be detected only in the flexion-extension scenario for both sensors, and in the hamstring curl and squat rotation scenarios for the shank and thigh sensor, respectively. The number of selected features goes from the 13 (in the walking sets) to 24 (in the flexion-extension scenario) in respect to the initial 64 considered in this category.

Regarding the jerk-based category, the exercises that show an improvement of the patient related to the shank sensor are the hamstring curl, flexion-extension, and walking at 3 km/h. On the other hand, a decline of the score is detected also in walking at 4 km/h for the thigh sensor, and in the squat rotation scenario for both sensors. The exercises that present the lowest number of features to assess the patient's progression along the rehab program are squat rotation and walking at 4 km/h which select the DSJ over one and two axis, respectively.

Finally, in the case of info/theoretical and spectral features a minimum number of 27 features is necessary for defining a decreasing trend in both hamstring curl and flexion-extension scenarios. The most selected features are LZC, SC, LFP, MFP, 3rd Quartile, and DMW.

Having a look at the scores of every category, it could be seen that even when the trend is decreasing it is not monotonic. Thus, important improvement of patient's knee health could be seen immediately after the surgery, while a jagged trend and a little progression characterise the last phase of the rehab program.

The application of mental distractions during the last two sessions seems to have no influence in the outcome. Further tests and analysis on right and left leg to assess if the application of mental distractions could affect the performance of the proposed scenarios should be evaluated.

Regarding the Single leg wall slide (SLWL), the proposed method helps in quantifying the muscle control of the patient. A high smoothness of the signal is

detected in case of regular standing executed by the thigh, getting into more dispersed distribution in case of low muscle control.

The results show an improvement patient's muscle control on both legs testified by reduced values of the radius along the 4^{th} sessions, and thus, more concentrated distributions.

CHAPTER 8

Conclusion

This thesis proposed the use of WIMUs for developing an objective evaluation that could support the clinical assessment of the knee health status. The use of inertial sensing platforms reveals to be a low-cost, practical and accurate solution in respect to the gold-standard systems. The proposed algorithm is able to detect the widest range of features and to select the most informative ones by combining the application of the Bhattacharyya distance (D_B) with a weighted K-means technique based on the Coefficient of Variation (CVV).

The patient's progression is more evident in the scenarios that have been tested from the pre- to post-surgery period. While, in the case of walking sets a flatter trend testifies on a relative improvement during the last sessions.

The number and type of chosen features varies on the different scenarios, overall, the most selected ones are GCT, RAV, Fluency over y-axis, KV, ROM over the x- and y-axis, LZC, SC, LFP, MFP, 3rd Quartile, and DMW.

The application of mental distractions

The use of D_B followed by CVV for defining a score indicator that classify the patient's performance, to the author's knowledge, have not been proposed in previous ACLR analysis.

Future developments are currently under study for grouping all the categories' indicators into a single score that allows the definition of patient's performances in respect to different scenarios.

Furthermore, other classification techniques which takes into account also the biological meaning of each feature can be compared to the proposed method for obtaining a more significant score indicator.

In the future, this score indicator could be transferred to a smartphone application for giving a feedback to the patients about at-home rehab.

Finally, the method proposed for analysing the Single Leg Wall Slide (SLWS) can help in detecting improvement in the muscle control of the quadriceps, even if more tests are needed to validate these results.

In conclusion, the use of the WIMUs and the proposed analysis proved to define a wide range of metrics and accurate methods that could support the clinical assessment during both typical scenarios of literature (e.g. hamstring curl, flexion-extension and walking sets) and new scenarios suggested by experts (e.g. Squat rotation and Single Leg Wall Slide), making the findings of this work a further step towards to the definition of an objective assessment of impaired subjects during ACLR.

Bibliography

[1] S. Bollen et al., “Epidemiology of knee injuries: diagnosis and triage”, 2000, Br J Sports Med 34: 227-8

[2] C. Walker et al., “A Patient Guide to Anterior Cruciate Ligament Reconstruction”, 2013

[3] R. Rafeeuddin et al., “Mapping current research trends on neuromuscular risk factor of non-contact ACL injury”, 2016

[4] C. Prodromos, “The Anterior Cruciate Ligament: Reconstruction and Basic Science”, 2017, page 66

[5] M. DiFabio et al., “Relationships of Functional Tests Following ACL Reconstruction: Exploratory Factor Analyses of the Lower Extremity Assessment Protocol”, 2017

[6] O. Olsen et al., “Exercises to prevent lower limb injuries in youth sports: cluster randomised controlled trial”, 2005

[7] J. Hertel et al., “A rehabilitation paradigm for restoring neuromuscular control following athletic injury”, 1998, Athletic Therapy Today 3 (5): 13-14

[8] M. Risberg, “We Need to Implement Current Evidence in Early Rehabilitation Programs to Improve Long-Term Outcome After Anterior Cruciate Ligament Injury”, 2016

[9] T. E. Hewett et al., “Biomechanical Measures of Neuromuscular Control and Valgus Loading of the Knee Predict Anterior Cruciate Ligament Injury Risk in Female Athletes”, 2005

[10] S. Campo, “Effects of lower-limb plyometric training on body composition, explosive strength, and kicking speed in female soccer players”, 2009

[11] E. Turner, “Female Soccer: Part 2— Training Considerations and Recommendations”, 2013

[12] T. N. Lindenfeld et al., “Incidence of Injury indoor soccer”, 1998

[13] K. R. Ford, “Valgus Knee Motion during Landing in High School Female and Male Basketball Players”, 2003

[14] L. E. Stanley, “Sex Differences in the Incidence of Anterior Cruciate Ligament, Medial Collateral Ligament, and Meniscal Injuries in Collegiate and High School Sports”, 2016

[15] G. D. Myer, “The Relationship of Hamstrings and Quadriceps Strength to Anterior Cruciate Ligament Injury in Female Athletes”, 2009

[16] https://www.mayoclinic.org/diseases-conditions/acl-injury/symptoms-causes

[17] D. Adams et al., “Current Concepts for Anterior Cruciate Ligament Reconstruction: A Criterion–Based Rehabilitation Progression, 2012

[18] R. Marks, “Knee Osteoarthritis and Exercise Adherence: A Review”, 2012

[19] F. Della Villa et al., “Anterior cruciate ligament reconstruction and rehabilitation: predictors of functional outcome”, 2015

[20] K. E. M. Harmelink et al., “The effectiveness of the use of a digital activity coaching system in addition to a two-week home-based exercise program in patients after total knee arthroplasty: study protocol for a randomized controlled trial”, 2017

[21] T.B. Almeida, “Evaluation of functional rehabilitation physiotherapy protocol in the postoperative patients with anterior cruciate ligament reconstruction through clinical prognosis: an observational prospective study”, 2016

[22] F. Lee et al., “Effects of a tailor-made exercise program on exercise adherence and health outcomes in patients with knee osteoarthritis: a mixed-methods pilot study”, 2016

[23] R. Houmanfar et al., “Movement Analysis of Rehabilitation Exercises: Distance Metrics for Measuring Patient Progress”, 2014

[24] S. V. Grinsven, “Evidence-based rehabilitation following anterior cruciate ligament reconstruction, 2010

[25] E. Dunphy et al., “Taxonomy for the Rehabilitation of Knee Conditions (TRAK), a Digital Intervention to Support the Self-Care Components of Anterior Cruciate Ligament Rehabilitation:Protocol of a Feasibility Study”, 2016

[26] https://www.buzzle.com/articles/how-to-use-a-goniometer.html

[27] http://www.australasianmedical.com.au/range-of-motion/inclinometers

[28] P. M. Mills, “Repeatability of 3D gait kinematics obtained from an electromagnetic tracking system during treadmill locomotion”, 2007

[29] http://lauflabor.ifs-tud.de/doku.php?id=facilities:kistler

[30] Z.C. On, “Development of an economic wireless human motion analysis device for quantitative assessment of human body joint”, 2017

[31] https://www.asc.ohio-state.edu/price.566/courses/BVE/joy.html

[32] G. Bonora et al., “Gait initiation is impaired in subjects with Parkinson’s disease in OFF state: Evidence from the analysis of the anticipatory postural adjustments through wearable inertial sensors, 2016

[33] Shi-Wei Mo et al. “Evaluation of the accuracy of gait events detected using three different methods during running”, 2017

[34] C. N. Teague, “Wearable knee health rehabilitation assessment using acoustical emissions”, 2017

[35] G. D. Meyer et al., “Neuromuscular training improves performance and lower-extremity biomechanics in female athletes”, 2005

[37] http://accessphysiotherapy.mhmedical.com/

[37] https://lmam.epfl.ch/page-73893-en.html

[38] M. Benoussaad et al., “Robust Foot Clearance Estimation Based on the Integration of Foot-Mounted IMU Acceleration Data”,2016

[39] A.W. K. Lam et al., “Improving Rehabilitation Exercise Performance through Visual Guidance, 2014

[40] S. Spasojević et al., “Combined Vision and Wearable Sensors-based System for Movement Analysis in Rehabilitation”, 2017

[41] F. Jin et al. “An estimation of knee and ankle joint angles during extension phase of standing up motion performed using an inertial sensor”, 2017

[42] F.J. Flores et al., “Validity and reliability of a 3-axis accelerometer for measuring weightlifting movements”, 2016

[43] P. Huynh et al., “VLC-Based Positioning System for an Indoor Environment Using an Image Sensor and an Accelerometer Sensor”, 2016

[44] https://www5.epsondevice.com/en/information/technical_info/gyro/

[45] Y. Wang, “Wearable Motion Sensing Devices and Algorithms for Precise Healthcare Diagnostics and Guidance”, 2015

[46] N. Ahmad, “Reviews on Various Inertial Measurement Unit (IMU) Sensor Applications”, 2013

[47] A. Frangi et al., “Z-Axis magnetometers for MEMS Inertial Measurement Units using an industrial process”, 2013

[48] https://www.alliedmarketresearch.com/accelerometer-and-gyroscope-market

[49] A. Lawrence, “Gyro and Accelerometer Errors and Their Consequences”. In: Modern Inertial Technology. Springer, New York, NY, 1993

[50] W. Johnston et al., “Objective classification of dynamic balance using a single wearable sensor”, 2016

[51] D. Whelan, “Evaluating Performance of the Lunge Exercise with Multiple and Individual Inertial Measurement Units”, 2016

[52] R. Zhu et al., “Realtime articulated human motion tracking using tri-axis inertial/magnetic sensors package”, 2004, IEEE Transactions on Neural Systems and Rehabilitation Engineering, 12:295–302

[53] A.S. Kund et al., “Hand Gesture Recognition Based Omnidirectional Wheelchair Control Using IMU and EMG Sensors”, 2017

[54] A. Tognetti et al., “Wearable Goniometer and Accelerometer Sensory Fusion for Knee Joint Angle Measurement in Daily Life”, 2015

[55] V. Agostini et al., “Instrumented gait analysis for an objective pre-/postassessment of tap test in normal pressure hydrocephalus”, 2015

[56] C. Buckley et al., “Quantification of upper body movements during gait in older adults and in those with Parkinson’s disease: impact of acceleration realignment methodologies”, 2017

[57] A. Sant’ Anna et al., “Assessment of Gait Symmetry and Gait Normality Using Inertial Sensors: In-Lab and In-Situ Evaluation”, 2013

[58] D. Novak et al., “Automated detection of gait initiation and termination using wearable sensors”, 2013, Med. Eng. Phys., v. 35, no. 12, pp. 1713–1720

[59] A. Laudanski et al., “A concurrent comparison of inertia sensor-based walking speed estimation methods”, 2011

[60] L. Nava et al., “Estimation of temporal gait parameters using Bayesian models on acceleration signals, 2015

[61] S. Tedesco et al., “Experimental Validation of the Tyndall Portable Lower-Limb Analysis System with Wearable Inertial Sensors”, 2016

[62] https://www.invensense.com/products/motion-tracking/9-axis/mpu-9250/

[63] https://developer.arm.com/products/processors/cortex-m/cortex-m4

[64] https://researchdesignlab.com/stm32-arm-cortex-m4-development-boardstm32f407vet6.html

[65] www.biomech.uottawa.ca/english/teaching/apa6905/lectures

[66] https://www.shutterstock.com/image-illustration/bones-lower-limbs-3d

[67] T. Seel, “Joint Axis and Position Estimation from Inertial Measurement Data by Exploiting Kinematic Constraints”, 2011

[68] Seel et al., IMU-Based Joint Angle Measurement for Gait Analysis, 2014

[69] O.H. Madgwic et al., “Estimation of IMU and MARG orientation using a gradient descent algorithm Sebastian”, 2011

[70] Q.Li et al.,”Walking speed estimation using a shank-mounted intertial measurement unit”, 2010

[71] Rinat Khusainov**,** “Real-Time Human Ambulation, Activity, and Physiological Monitoring: Taxonomy of Issues, Techniques, Applications, Challenges and Limitations”, 2013

[72] E. Sejdic, et al., “A comprehensive assessment of gait accelerometry signals in time, frequency, and time-frequency domains,” IEEE Trans Neural Systems Rehabilitation Eng, 22(3), 603-612, 2014.

[73] F. Riva, et al., “Estimating fall risk with inertial sensors using gait stability measures that do not require step detection,” Gait Posture, 38, 170–174, 2013.

[74] M. Kojima, et al., “Power spectrum entropy of acceleration time-series during movement as an indicator of smoothness of movement,” J Physiol Anthropol., 27(4), 193-200, 2008.

[75] M. Gietzelt, “A clinical study to assess fall risk using a single waist accelerometer”, 2009

[75] M. Aboy, “Interpretation of the Lempel-Ziv Complexity Measure in the Context of Biomedical Signal”, 2006

[76] Y. Zhang, “Using Lempel–Ziv Complexity to Assess ECG Signal Quality”, 2016

[77] https://www.bistasolutions.com/resources/blogs/statistical-outliers-detection-treatment/

[78] D. Schwender, “Spectral edge frequency of the electroencephalogram to monitor depth of anaesthesia with isoflurane of propofol”, 1996

[79] N. Hogan, “Sensitivity of Smoothness Measures to Movement Duration, Amplitude and Arrests”, 2009

[80] http://www.militarydisabilitymadeeasy.com/kneeandleg.html

[81] https://www.slideshare.net/SebastianRaschka/nextgen-talk-022015/9 UnsupervisedlearningSupervisedlearningClusteringDBSCAN_on_a_toy_datasetClassicationSVM

[82] E. Ficarra, Bioinformatic course, Politecnico of Turin a.a.2016/2017

[83] Liu et al., “Simplest representation yet for gait recognition: average silhouette”, 2004

[84] G.B. Coleman, “Image Segmentation by Clustering”, 1979

[85] C.You et al., “A GMM supervector kernel with the Bhattacharyya distance for SVM based speaker recognition

[86] C. Mahalanobis, “On a generalized distance in statistics”, 1986

[87] B. Bhattacharyya, “On a measure of divergence between two statistical populations defined by their probability distributions”,1943

[88] https://misti.com/infosec-insider/artificial-threat-intelligence-using-data-science-to-augment-analysis

[89] H. Wu et al., “Spectral Ensemble Clustering via Weighted K-Means: Theoretical and Practical Evidence”, 2017

[90] S. Tedesco et al., “Metrics for monitoring patients progress in a Rehabilitation context: A case study based on Wearable Inertial Sensors”, 2018

[91] S. Fong et al., “A Novel Feature Selection by Clustering Coefficients of Variations”, 2014

[92] R. Ganea et al., “Multi-parametric evaluation of sit-to-stand and stand-to-sit transitions in elderly people”, 2011

Ringraziamenti

Ho sempre creduto che quello che siamo e che diventiamo non dipenda soltanto da noi, ma sia frutto del contributo di ogni singola persona che incrocia il nostro cammino.

Ringraziare ufficialmente non è probabilmente nella mia indole, ma credo che sia giusto dare i meriti a chi in questa vita, in questo percorso e in quest'ultimo capitolo di studi mi ha portato ad essere dove e chi sono oggi.

Il mio "grazie" più grande va ai miei genitori, per avermi dato sempre la possibilità di scegliere il mio futuro senza vincoli, per gli innumerevoli "ce la puoi fare", e per quell'espressione piena di gioia e fierezza ad ogni buono, seppur piccolo risultato.

Grazie a mio fratello, per essere da una vita e per la vita la risata che mi salva la giornata. Ai miei nonni, per quel "tieni alta la bandiera e fai vedere chi sei" tra la commozione di una partenza e di un successo. E a mio zio Ciro, per avermi insegnato a non vivere una battaglia persa come una sconfitta definitiva, ma soltanto come una caduta in un lungo percorso.

Grazie a coloro che mi hanno permesso di fare quest'esperienza irlandese. Al mio professore Danilo, per aver dimostrato, in aggiunta alle conoscenze personali, una cordialità e un'umanità rare da trovare in ambito universitario. A Brendan, "for the support and guidance during the whole experience in Tyndall". E a Salvatore, un supervisor in apparenza severo e fiscale (molto fortunato nelle partite di biliardino) che con le sue parole e non parole è riuscito a insegnarmi tanto.

Grazie alla mia famiglia torinese.

A Lu, Viviana e Davide, per aver sopportato più di ogni altro tutta la mia ansia&sapone, per aver sempre lasciato un posto per me (possibilmente vicino alla porta quando ero in ritardo a lezione), e per aver reso quel Polito uno dei ricordi più belli che ho.

Ad Emma, la persona più determinata che conosca, per tutto "L'ov" che mi dimostra ogni giorno. A Claudia e Luigi, per il loro cuore grande e per tutte le volte che mi hanno adottato per un pranzo domenicale. A Laura, per aver portato un po' di napoletanità a Corso Duca e per quei sabati in sessione in cui l'unica consolazione era un "sei bellissima, troverai". Ad Antonella e Imma, per essermi state accanto in quella folle "Turin Express" e per tutta quella serie di divertenti e sfortunati eventi che si scagliavano su Casa Papetti tra un esame e l'altro. A Chiara e Federica, per la fantastica esperienza di convivenza dell'ultimo anno, per gli abbracci (in quantità industriali) e per avermi strappato un sorriso anche nei momenti più disperati distese su un letto a "quattro di bastoni".

Grazie al gruppo italiano di Cork che con le sue tradizioni consolidate ("Venerdì Crane Lane" o "stasera pizza") mi ha fatto percepire il calore del Sud nei giorni di pioggia irlandese. E grazie alla piccola minoranza non italiana che ha tenuto allenato il mio inglese. "I would especially like to thank Nektaria, for the kindness she has showed me since the first day she came, for her generous support, and for the hilarious moments we spent outside of the office. Then, I would like to thank Niamh, a list-addicted girl that is affected (unfortunately for her, but likely for me) by ACL becoming the best patient and Irish friend I could ever had".

Grazie a quelle persone che a poco a poco si sono fatte spazio nella mia vita diventando importanti. A Simona, una persona tutta "anima e cuore", per avermi dimostrato che i rapporti possono andare oltre le distanze e che ci sarà sempre un posto ad accogliermi in caso di necessità.

E a Teresa, il pezzo d'Irlanda che mi mancherà di più, che da quel "Sei italiana? Cosa hai scritto qui?" nel bel mezzo di un'induction, ha riempito le mie giornate a Cork con la sua semplicità.

L'ultimo ringraziamento va a coloro che conoscono ogni mia smorfia, ogni mia esperienza o pensiero: le mie persone del cuore.

Grazie a Gabriella, Manuela e Marina, che riescono da una vita ad incastrare i progetti di quelle liceali che sono ormai donne. Siete nella maggior parte dei miei ricordi, dalle riunioni d'emergenza improvvisate per ogni tipico problema adolescenziale, a quelli più commoventi, in cui abbiamo condiviso la gioia di una laurea, di un matrimonio o di una gravidanza. Sarete sempre il mio punto di riferimento indipendentemente dall'angolo di mondo in cui mi troverò.

E infine, grazie a Morena, ex-coinquilina, collega e amica che ogni giorno mi contagia con la sua leggerezza. A lei che prevede ogni mia espressione e che riesce a stordirmi con quella vocina quando non vede l'ora di raccontare qualcosa. A lei che è la mia casa in ogni momento di instabilità o incertezza e che mi ricorda che "tutto sommato la vita è bella così".